Mo et al. Cell Communication and Signaling (2025) 23:280
https://doi.org/10.1186/s12964-025-02289-7

Cell Communication and Signaling

RESEARCH Open Access

Activation of mechanosensitive ion channel Piezo1 linking metabolic reprogramming and pro-inflammatory responses in hepatocellular carcinoma

Juanfen Mo[1†], YuXuan Zhang[1†], Chenxi Cao[2†], WeiLi Zheng[1], Li Zheng[1], Xiaoguang Wang[3], Shiyue Wang[1], Jiayuan Wu[1*] and Yi Bao[1,2,4*]

Abstract

Piezo1 is identified as a novel mechanosensitive ion channel protein regulating a variety of physiological and pathological processes. However, the cellular effects of activation of Piezo1 protein on hepatocellular carcinoma (HCC) remains to be illuminated. In this study, we investigated the interaction between Piezo1 activation associated with metabolic reprogramming, pro-inflammatory cytokine release, and HCC progression. Our results indicated that the expression of Piezo1 gene and protein was up-regulated in the cancerous tissues of HCC patients, and the increased mRNA levels of Piezo1 were associated with unfavorable clinical outcomes. The activation of Piezo1 by its agonist Yoda1, facilitated HCC development by stimulating proliferation, migration, and invasion. Furthermore, Piezo1 channel activation by its agonist mediated pro-inflammatory responses mainly through its downstream molecule CXCL8 via ERK1/2 and AKT signaling pathways by up-regulating CXCL8 expression in transcriptional levels of HCC cells. The secretion of CXCL8 was induced by Piezo1 activation in HCC cells, improving immune cells trafficking and promoting angiogenesis, and therefore cross-talked with the tumor microenvironment (TME). Additionally, increased expression of MTHFD2, a metabolic checkpoint enzyme, was induced by the activation of Piezo1 channel and was likely to be a downstream target involved in mitochondrial stress followed by Piezo1 channel activation. In vitro data was further corroborated by the deceleration of tumor growth sizes in nude mice subcutaneously injected with Piezo1-depleted HCC cells in vivo. Finally, we showed synergistic anti-tumor effects of GsMTx4 and arachidonic acid, two Piezo1 antagonists, together with oxaliplatin in HCC cells. In summary, our findings suggest that the present linkage of metabolic reprogramming and pro-inflammatory responses after Piezo1 activation in HCC. Targeting Piezo1 appears to be a novel therapeutic strategy improving the treatment efficacy in HCC.

†Juanfen Mo, YuXuan Zhang and Chenxi Cao contributed equally to this work.

*Correspondence:
Jiayuan Wu
wujiayuan@zjxu.edu.cn
Yi Bao
ybao2011@zjxu.edu.cn

Full list of author information is available at the end of the article

Keywords Hepatocellular carcinoma, Piezo1, CXCL8, MTHFD2, Mitochondria

Graphical Abstract

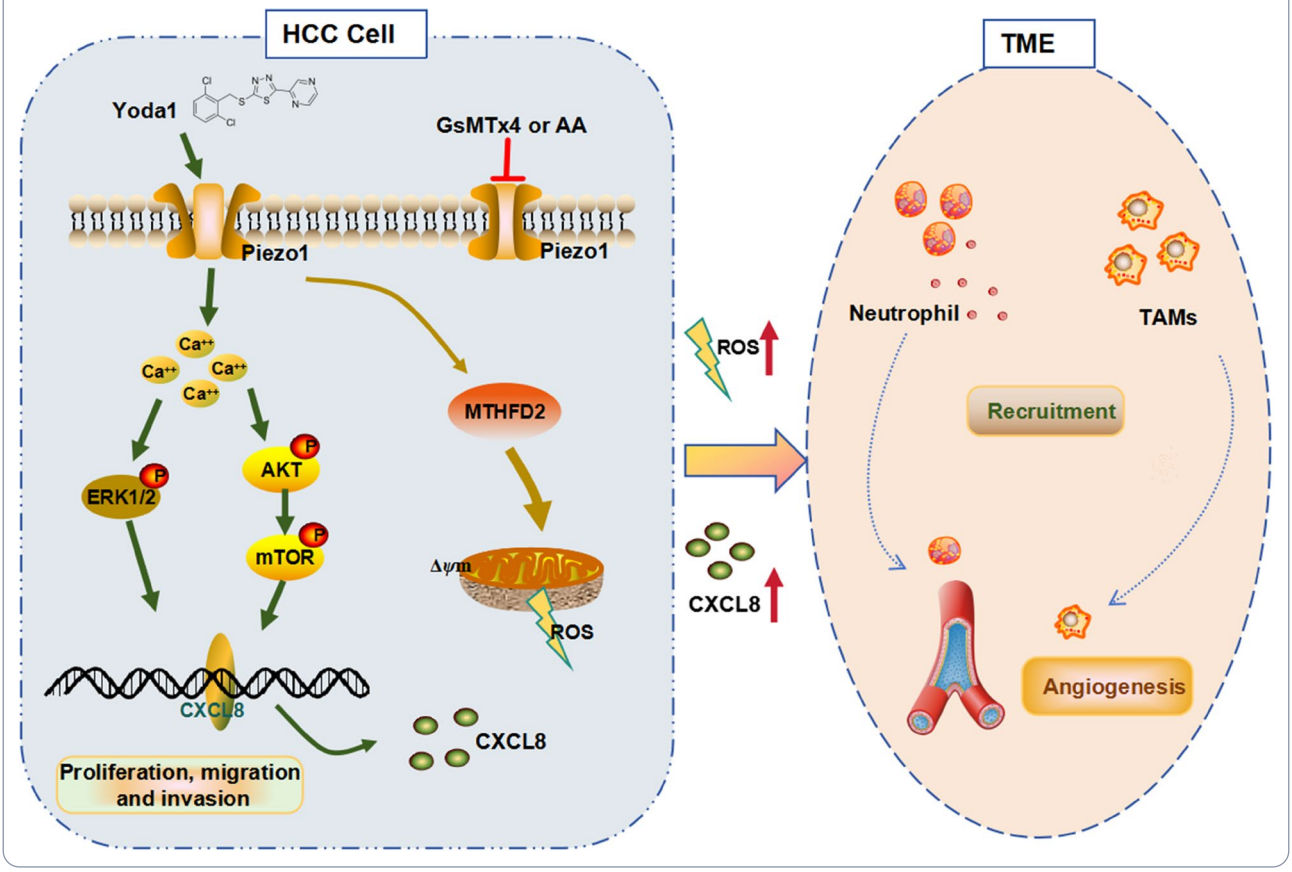

Introduction

Hepatocellular carcinoma (HCC), a third leading cause of cancer-related death worldwide [1], typically derives from an inflammatory environment at the liver tissues. For instance, the higher incidences of chronic hepatitis B virus (HBV) infection in South Asia [2], and nonalcoholic fatty liver disease (NAFLD) and nonalcoholic steatohepatitis (NASH) in the developed countries [3], all markedly contribute to the development of HCC.

Progressive hepatic fibrosis is a prevalent consequence across all types of chronic liver diseases and correlates with the development of HCC [4]. During the persistent chronic inflammatory environments at the liver tissues, a variety of immune cells, such as monocyte-derived macrophages, are recruited into the intrahepatic micro-environment, which leads to the dysfunction of resident cells, for instance, Kupffer cells, hepatic stellate cells (HSCs), and stromal cells within liver tissues, which alternatively serve as a potent impetus for remodeling of liver matrix, thereby exacerbating liver fibrosis and cirrhosis [5]. Hepatic fibrogenesis, which entails the eventual reconstruction of the intrahepatic structure [6–8], may affect mechanosensitive receptors on the cell surface of hepatocytes. The transduction of mechanical stimuli, including stretching, compression, and shear stress, into electrical signals mediates a complex cascade of intracellular events [9]. Among these mechanosensitive receptors, a tremendous focus has been placed on the exploration of Piezo1, derived from a Greek word "piezein," means "pressure," which was discovered in 2010 [10]. In the following studies, Piezo1 approves to be a crucial mechanosensitive ion channel protein playing fundamental roles in various biological processes by converting mechanical stimuli into cellular signals [11]. Emerging evidences also further implicate the possible involvement of Piezo1 activation in the pathogenesis of renal fibrosis, pulmonary fibrosis, cardiac fibrosis, pancreatic fibrosis, as well as multiple malignancies [12–14]. However, in HCC patients coupled with fibrosis or cirrhosis, the operating roles of Piezo1 in the advancement of HCC remains unclear.

In the present study, we revealed that Piezo1 was up-regulated in tumor tissues of HCC, and higher mRNA levels of Piezo1 were associated with unfavorable prognosis. The activation of Piezo1 ion channel affected several

cellular events such as improved cell proliferation, migration, and invasion. Mechanically, increased mitochondrial one-carbon enzyme MTHFD2 induced by Piezo1 channel opening was likely to be the downstream molecule that orchestrated the metabolic remodeling in the liver cancer cells. Importantly, enhanced CXCL8 released by tumor cells after Piezo1 activation is characterized as a crucial pro-inflammatory cytokine in the crosstalk with the tumor microenvironment (TME). Finally, our study suggested that blocking the Piezo1 channel with its inhibitors or antagonists together with oxaliplatin conferred therapeutic advantages in HCC.

Materials and methods

Tumor tissue samples

A total of fifteen paired cancerous tissues and paracancerous tissues from HCC patients were collected from the Second Affiliated Hospital of Jiaxing University. Among these tissues, seven fresh pairs of cancerous tissues and paracancerous tissues were used for a western blot analysis, and eight pairs of paraffin-encapsulated cancerous tissues and paracancerous tissues (2 cm away from the edge of the tumor) from patients who underwent radical hepatectomy were used for an immunohistochemistry (IHC) study. Clinical pathological parameters were retrieved from medical records, and among these patients, eleven cases were males (73.3%) and four cases were females (26.7%) with an average age of 60 years (range: 37–83 years).

The pathological stages were determined according to the 8th edition AJCC-TNM staging system with stage I ($N=7$, 46.7%), II ($N=2$, 13.3%) and III ($N=6$, 40.0%) respectively. Serum samples were obtained from twenty patients with advanced HCC and sixteen healthy donors as controls used for an enzyme-linked immunosorbent assay (ELISA) study. Peripheral blood mononuclear cells (PBMCs) were isolated from peripheral blood of six healthy donors used for chemotaxis assays. Each tumor tissue diagnosed as HCC was histologically confirmed by experienced pathologists. Serum samples were obtained from healthy donors at our medical center. Written informed consents were obtained from all patients recruited in this study. Each procedure was conducted according to the Declaration of Helsinki and approved by the Ethics Committee of the Second Affiliated Hospital of Jiaxing University (Ethics No: JXEY-2023SZ019).

Bioinformatics data extraction and analysis

The gene expression data generated from HCC patients (374 tumor cases and 50 paracarcinoma tissues, data type: HTSeq-FPKM) were downloaded from the TCGA database (https://portal.gdc.cancer.gov/). R software (version 4.3.2) was utilized for statistical analysis, and the results were visualized using box plots.

Protein array data including serum CXCL8 concentrations were retrieved from a Gene Expression Omnibus (GEO) database (GSE261672), which was generated by a Luminex assay using serum specimens originally obtained from 96 cases of patients with treatment-naïve unresectable HCC (uHCC) and 20 cases of cancer-free chronic liver disease (CLD) as controls [15].

Cell lines and chemical compounds

Three HCC cell lines, including Huh7, HepG2, and Hep3B, as well as a human umbilical vein endothelial cells (HUVEC) line were obtained from the Cell Bank of Type Culture Collection of Chinese Academy of Sciences (China). All cell lines were cultured in Dulbecco's Modified Eagle's Medium (DMEM, Solarbio, China) containing 10% FBS (Gibco, New Zealand) and 100 μg/mL penicillin/streptomycin (Sorlarbio, China) at 37℃ with 5% CO_2.

Yoda1 (#HY-18723, MedChemExpress, USA), a specific Piezo1 agonist, was used at 10 μM concentrations in the cell culture studies. A highly selective ERK1/2 inhibitor, SCH772984 (1 μM) (#HY-50846, MedChemExpress, USA), and an AKT inhibitor, MK-2206 (10 μM) (#HY-10358, MedChemExpress, USA), were used for assays blocking these enzymes' activities. GsMTx4 (#HY-P1410, MedChemExpress, USA), a spider venom peptide that selectively inhibits Piezo1, was used at 5 μM concentration in the cell culture studies. Arachidonic acid (AA, #HY-10863, MedChemExpress, USA), an essential polyunsaturated fatty acid, is found to inhibit the Piezo1 channel reported by a previous literature [16]. Oxaliplatin (2 μM) (#HY-17371, MedChemExpress, USA), a standard chemotherapeutic drug used in the treatment of advanced HCC, was studied in the synergistic antitumor effects together with targeting Piezo1 in cell culture studies.

Immunohistochemistry

The expression of Piezo1 and its relevant proteins in the tumor tissues of HCC patients were examined by IHC analysis using formalin-fixed paraffin-embedded specimens. Briefly, paraffin-embedded tissues were cut into 5 μm slides. Tissues were incubated with anti-Piezo1 (#28511-1-AP, Proteintech, China, 1/200), anti-α-SMA (#14395-1-AP, Proteintech, China, 1/100), anti-CXCL8 (#94407T, Cell Signaling Technology, USA, 1/100), anti-MTHFD2 (#sc-100750, Santa Cruz, USA; 1/100), anti-VEGF-α (#19003-1-AP, Proteintech, China, 1/200) and anti-Ki67 antibodies (#27309-1-AP, Proteintech, China, 1/2000) overnight at 4 °C. Next day, each sample was incubated with a second antibody for 1 h. The expression signals were detected and analyzed by a light microscope (Zeiss, Germany). Slide staining was scored according to intensities under the light microscopy: 0 = background

staining intensity; 1 = weak staining intensity; 2 = moderate staining intensity; 3 = strong staining intensity. Histopathological evaluation was performed by two independent pathologists who were blinded to the clinical data of the cohort. Field selection was initiated with preliminary screening at low magnification (40×) to identify tumor cell-enriched regions. Subsequently, five non-overlapping fields were randomly selected to record the staining intensity of positively stained cells in tumor cells under high-power fields (200×).

Western blot and antibodies

Cancerous and paracancerous tissues from HCC patients, as well as HCC cells, were lysed using RIPA lysis buffer (#R0010, Solarbio, China) supplied with 1 mM PMSF. Approximately 20 μg of lysate was separated on a SurePAGE™ precast Bis-Tris 4–20% gradient gel (#M00657, Genscript, China) and subsequently transferred onto a 0.45 μm PVDF membrane (#IPVH00010, Merck, USA). The membrane was blocked with 5% non-fat milk powder in TBST buffer for 1 h on an orbital shaker and then incubated with the following primary antibodies overnight at 4 °C: Piezo1 (#28511-1-AP, Proteintech, China; 1/1000), Piezo2 (#26205-1-AP, Proteintech, China; 1/1000), CXCL8 (#94407, Cell Signaling Technology, USA; 1/500), E-cadherin (#3195, Cell Signaling Technology, USA; 1/500), p-ERK1/2 (#4370, Cell Signaling Technology, USA; 1/3000), ERK (#4695, Cell Signaling Technology, USA; 1/2000), p-AKT (#4060, Cell Signaling Technology, USA; 1/2000), AKT (#4691, Cell Signaling Technology, USA; 1/2000), p-mTOR (#5536, Cell Signaling Technology, USA; 1/500), mTOR (#2983, Cell Signaling Technology, USA; 1/500), MTHFD2 (#sc-100750, Santa Cruz, USA; 1/200), α-tubulin (#3873, Cell Signaling Technology, USA; 1/2000) and β-actin (#E021020, EarthOX, USA; 1/2000). Next day, the membrane was washed by TBST and then incubated with goat anti-mouse or anti-rabbit IgG HRP-conjugated secondary antibodies (Jackson Immuno Research, USA; 1/5000) for 90 min, followed by ECL development (#WBKLS0500, Merck, USA). Specific protein expression bands and image analysis were performed using Image Lab 3.0 software (Bio-Rad, USA).

Enzyme-linked immunosorbent assay (ELISA)

ELISA was performed to detect circulating CXCL8 (Proteintech, China) secreted in human serum samples and supernatants obtained after culturing Huh7 and HepG2 cells. ELISA experiments were performed according to the manufacturer's instructions. The optical density (OD) value was determined at 450 nm by a microplate reader (Thermo Fisher Scientific, USA).

Intracellular calcium influx analysis

Both Huh7 and HepG2 cells were treated with Yoda1 in 24-well plates for 0, 5 min, 30 min, 1 h, 4 h, and 24 h, respectively, and then loaded with a Fluo-4 Calcium Assay Kit (Fluo-4 AM) (Beyotime, China) according to the manufacturer's guidelines at 37 °C for approximately 30 min. Intracellular calcium influx was observed with a fluorescence microscope (LEICA DMi8, Germany) and images were recorded by Leica Application Suite X software (LEICA, Germany). The fluorescence value was analyzed by ImageJ software.

Cell proliferation assay

Cell proliferation was detected by flow cytometry using an AlexaFluor-488 anti-BrdU antibody (Abcam, USA) and Cell Titer-Glo® luminescent kit (Promega, USA). In the Brdu assay, 1×10^6 Huh7 and HepG2 cells were collected and resuspended in 1 × binding buffer followed by incubation with 10 μL of each antibody for 15 min in a dark environment at room temperature. Flow cytometry analysis was performed on a BD FACS Canto II machine (BD, USA) and analyzed by FlowJo software (V.7.6.1, Tree Star, USA). In the Cell Titer-Glo® luminescent assay, cells were seeded in 96-well plates at 1×10^4 cells/well and treated with or without Yoda1 for 24 h. A 100-μL volume of assay reagent was added to each well, and the density of fluorescence was measured by a Varioskan LUX Multimode Microplate Reader (Thermo Fisher Scientific, USA).

Cell apoptosis assay

Cell apoptosis was performed by a PI/Annexin V kit (BD Biosciences, USA). Cells were collected and resuspended in 1 × Binding Buffer followed by incubation with Annexin V for 20 min in dark. PI was added to each sample 5 min before detection. Flow cytometry analysis was performed on BD FACS Canto II machine with FACSDiva software (BD, USA).

Cell viability assay

Cell viability assay was performed by a CCK-8 kit (DOJINDO, Japan). Briefly, cells were incubated with 10 μL CCK-8 solution for 1 h at 37 ℃. The experimental procedure was conducted according to the protocol provided by the manufacturer. The absorbance of the cells was measured at 450 nm by a Multiskan GO Microplate Reader (Thermo, USA).

Wound healing assay

After Yoda1 treated the Huh7 and HepG2 cells for 24 h, cells grew to reach a tight cell monolayer in 12-well plates. The cell layer was scratched by a sterile 200 μL plastic pipette tip. Then cells were further washed twice with PBS and cultured in medium containing 1% FBS for

Table 1 mRNA primer sequences for quantitative PCR

Gene	Forward Sequence	Reverse Sequence
Piezo1	TTCCTGCTGTACCAGTACCT	AGGTACAGCCACTTGATGAG
CXCL8	CACTGCGCCAACACAGAAAT	GCCCTCTTCAAAAACTTCTCCAC
INHBA	CTCGGAGATCATCACGTTTG	CCTTGGAAATCTCGAAGTGC
IL-6	ACTCACCTCTTCAGAAC-GAATTG	CGGGCCGATTGATCTCAGC
VEGFA	TGCAGATTATGCGGATCAAACC	TGCATTCACATTTGTTGTGCT-GTAG
MMP1	ATGCTTTTCAACCAGGCCC	CAGTAGAATGGGAGAGTC
TNFA	AGGACACCATGAGCACT-GAAAGC	AAGGAGAAGAGGCTGAG-GAACAAG
TGFB1	CAATTCCTGGCGATACCTCAG	GCACAACTCCGGTGACATCA
CXCR1	CGCCATGGATTCCTCAAGAT	AGAGACATTGACAGAC-GAAGAAG
β-actin	GGATGCAGAAGGAGATCACTG	CGATCCACACGGAGTACTTG

24 h. The migrated cells at the wound front were immediately captured using a light microscope (Zeiss, Germany) and analyzed by the ImageJ software.

Transwell invasion assay

Cell invasion assay was conducted by using a transwell chamber (Corning, USA) with 1:8 diluted Matrigel matrix (Corning, USA). Huh7 and HepG2 cells were seeded into the upper chambers coated with serum-free medium, and 10% FBS-containing DMEM medium was placed in the bottom chamber. After 24 h, 4% paraformaldehyde (Beyotime, China) was added, and cells were fixed at room temperature for 30 min. Next, the cells were washed with PBS and stained with 0.1% crystal violet (Solarbio, China) for 30 min. A Carl Zeiss inverted microscope was used to count the cells in each field of view (Zeiss, Germany).

RNA extraction and RNA-sequencing analysis

Triplicate samples of Huh7 cells treated with DMSO or Yoda1 for 24 h were collected, and total RNA was extracted by TRIzol reagent (Invitrogen, USA). The quality RNA was examined and RNA sequenced by the Illumina Novaseq 6000 platform (Illumina, USA), which was provided by Hangzhou LC Bio Technology Co., Ltd. (China).

Real-time PCR

The extracted mRNA was reverse transcribed into cDNA using RT Master Mix reagent (Takara, Japan). qPCR amplification was performed in a Roche LightCycler® 480 machine (Roche, USA) with SYBR Green™ Premix Ex Taq™ II (Takara, Japan). Primers used in this study were listed in Table 1 (synthesized by Sangon Biotech, China). Each mRNA level was normalized to *β-actin* gene expression. Relative mRNA expression was calculated by the $2^{-\Delta\Delta Ct}$ method.

Table 2 siRNA sequences for transfection

Gene	Forward Sequence	Reverse Sequence
Piezo1-1#	GGGACUACUUCCUGUUUGATT	UCAAACAG-GAAGUAGUCCCTT
Piezo1-2#	GCCUCAUUCUGUACAACGUTT	ACGUUGUACA-GAAUGAGGCTT
Piezo1-3#	GCGUCUUCCUUAGCCAUUATT	UAAUGGCU-AAGGAAGACGCTT
MTHFD2	GCCUCUUCCAGAGCAUAUUTT	AAUAUGCUCUG-GAAGAGGCTT

siRNA transfection

Piezo1 siRNAs, MTHFD2 siRNAs and negative control siRNAs were designed and synthesized by GenePharma (China) as follows in Table 2. HCC cells were transfected by Lipofectamine RNAiMAX transfection reagent (Invitrogen, USA) and Opti-MEN (Invitrogen, USA) according to the manufacturer's instructions. After 48 h, the maximal silencing efficiency was evidenced by western blot analysis.

shRNA transfection

Piezo1 shRNA lentiviral vectors and negative control shRNA lentiviral vectors were designed and synthesized by GenePharma (China) as follows:

Piezo1-homo-1#: 5'-CGGCCCTGTGCATTGATTATC-3',

Piezo1-homo-2#: 5'-TGCGTCATCATCGTGTGTAAG-3',

Piezo1-homo-3#: 5'-CGAGATCTCGCACTCCATTAT-3'.

Huh7 cells were infected with lentiviral vectors for 24 h. Then, the cells were replaced with fresh medium and screened by 2 μg/mL puromycin (Solarbio, China) for another five days. The Piezo1 knockdown efficiency was determined by western blot.

Dual luciferase report assay

CXCL8 transcriptional activity was performed by a dual luciferase report assay. Briefly, Huh7 cells were transfected with 100 ng GPL4-Basic or GPL4-CXCL8 reporter plasmids (designed and constructed by GenePharma) for 48 h. Subsequently, cells were treated with or without Yoda1 (10 μM) for 24 h. The firefly and Renilla luciferase activities were measured by Dual Luciferase Reporter Assay kit (Promega, USA) using a Varioskan LUX Multimode Microplate Reader (Thermo Fisher Scientific, USA).

The effects of the inhibition of ERK1/2 and AKT enzyme activities on the regulation of CXCL8 expression at transcriptional levels were examined in the Huh7 cells transiently transfected with GPL4-Basic or GPL4-CXCL8 reporter followed by incubation with 1 μM SCH772984 (ERK1/2i) or 10 μM MK-2206 (AKTi) for 2 h. The Dual

Luciferase Reporter Assay was performed the same as above.

Chemotaxis assay

PBMCs were isolated from the peripheral blood of six healthy donors. PBMCs were seeded on a 24-well transwell plate with 3 μm pore polycarbonate membrane inserts (Corning, USA). 1×10^5 PBMC/well suspended in 200 μL RPMI 1640 (Solarbio, China) containing 0.5% FBS were placed in the upper chamber, and 600 μL RPMI 1640 containing 10% FBS, human recombinant CXCL8 protein (hrCXCL8, 10 ng/mL, 100 ng/mL and 1000 ng/mL) or 50 μL cell supernatants obtained from Huh7 cells incubated with Yoda1 (10 μM) for 24 h were added to the lower chamber. The migration of PBMCs from the upper chamber into the lower chambers was collected and counted after 6 h.

Tube formation assay

25 μL HUVEC cells (3×10^4 cells/well) were added to 96-well plates containing 25 μL Matrigel glue (Corning, USA) after being treated with 1% DMSO, 10 μM Yoda1, 100 ng/mL hrCXCL8 or conditioned medium collected from Huh7 cells incubated with Yoda1 (10 μM) for 8 h. Tube formation images were recorded by a microscope (Zeiss, Germany).

Measurements of intracellular ROS levels

Intracellular reactive oxygen species (ROS) was measured using a dichloro-dihydro-fluorescein diacetate (DCFH-DA) method [17]. In brief, cells were stained with 10 μM DCFH-DA working solution (Beyotime, China) for 20 min at 37 ℃. Images were captured and analyzed using a fluorescence microscope (Zeiss, Germany).

Mitochondrial membrane potential detection

Mitochondrial membrane potential was measured by a tetramethylrhodamine methyl ester (TMRM) probe [18]. TMRM (Bestbio, China) was added to the culture at a final concentration of 20 nM and incubated at 37 ℃ for 30 min. After staining, we replaced the staining solution with fresh culture medium and observed fluorescence under a fluorescence microscope (Zeiss, Germany).

Animal experiments

Five-week-old male BALB/c nude mice purchased from Changzhou Cavens Experimental Animal Co., Ltd. (Certification No. SCXK (Su) 2021-0013) were randomLy divided into the shVec group and the shPiezo1 group. There were at least 6 mice in each group ($n = 6$). All mice were raised in a specific pathogen-free environment. For the tumor xenograft experiment, stable shPiezo1-knockdown Huh7 cells or scramble shRNA control cells were inoculated subcutaneously into the flanks of nude mice (1×10^7 cells/100 μL/mouse). Caliper measurements began once tumors became visible. Tumor volumes were measured every 3 days until 4 weeks by caliper according to the formula $V = \text{length} \times \text{width}^2 / 2$. In our animal experiments, tumor mass formation strictly followed the NIH Guidelines for Endpoints in Animal Study Proposals (2019) [19]: tumor mass did not exceed 10% of normal mice body weight, and tumors on the body surface of adult mice did not exceed 20 mm in diameter in either direction. After 4 weeks, all mice were sacrificed, and subcutaneous tumor xenografts were dissected and fixed by 4% paraformaldehyde for hematoxylin-eosin (HE) staining and IHC experiments. All animal experimental procedures were operated in accordance with the institutional guidelines for animal care and approved by the Animal Ethical Committee of Jiaxing University (JUMC2022-101).

Statistical analysis

All statistical data were conducted using GraphPad Prism 6.0 software (GraphPad Software Inc., USA). Differences between two groups or multiple groups were determined using an unpaired *t* test or one-way ANOVA, respectively. For continuous variables, the data are presented as mean ± SD. Survival curves were plotted by a Kaplan-Meier method and compared by the log-rank test. Correlations were analyzed using the Spearman's rank correlation test. $P < 0.05$ was considered statistically significant.

Results

Piezo1 was highly expressed in the tumor tissues of HCC patients and predicted an unfavorable prognosis

We first detected the protein expression of Piezo1 in the cancerous tissues and paracancerous tissues from HCC patients by western blot and IHC assays, respectively. Elevated protein levels of Piezo1 were initially identified in HCC cancerous tissues compared to adjacent non-cancerous tissues using western blot analysis (Fig. 1A). Subsequent IHC analysis further confirmed that Piezo1 protein expression was statistically more pronounced in HCC tissues than in adjacent tissues ($P < 0.05$) (Fig. 1B). Moreover, bioinformatics analysis of HCC patient data from the TCGA database revealed that Piezo1 mRNA levels were significantly higher in tumor tissues compared to controls ($P < 0.05$) (Fig. 1C). However, no significant variation in Piezo1 gene expression was observed across the four stages of HCC as defined by the TNM classification system ($P > 0.05$) (Fig. 1D). Kaplan-Meier survival analysis showed that HCC patients with higher Piezo1 mRNA levels experienced reduced disease-free survival (DFS) and overall survival (OS) compared to those with lower Piezo1 expression (cutoff value 50%/50%: the expression levels above the median were classified as high expression

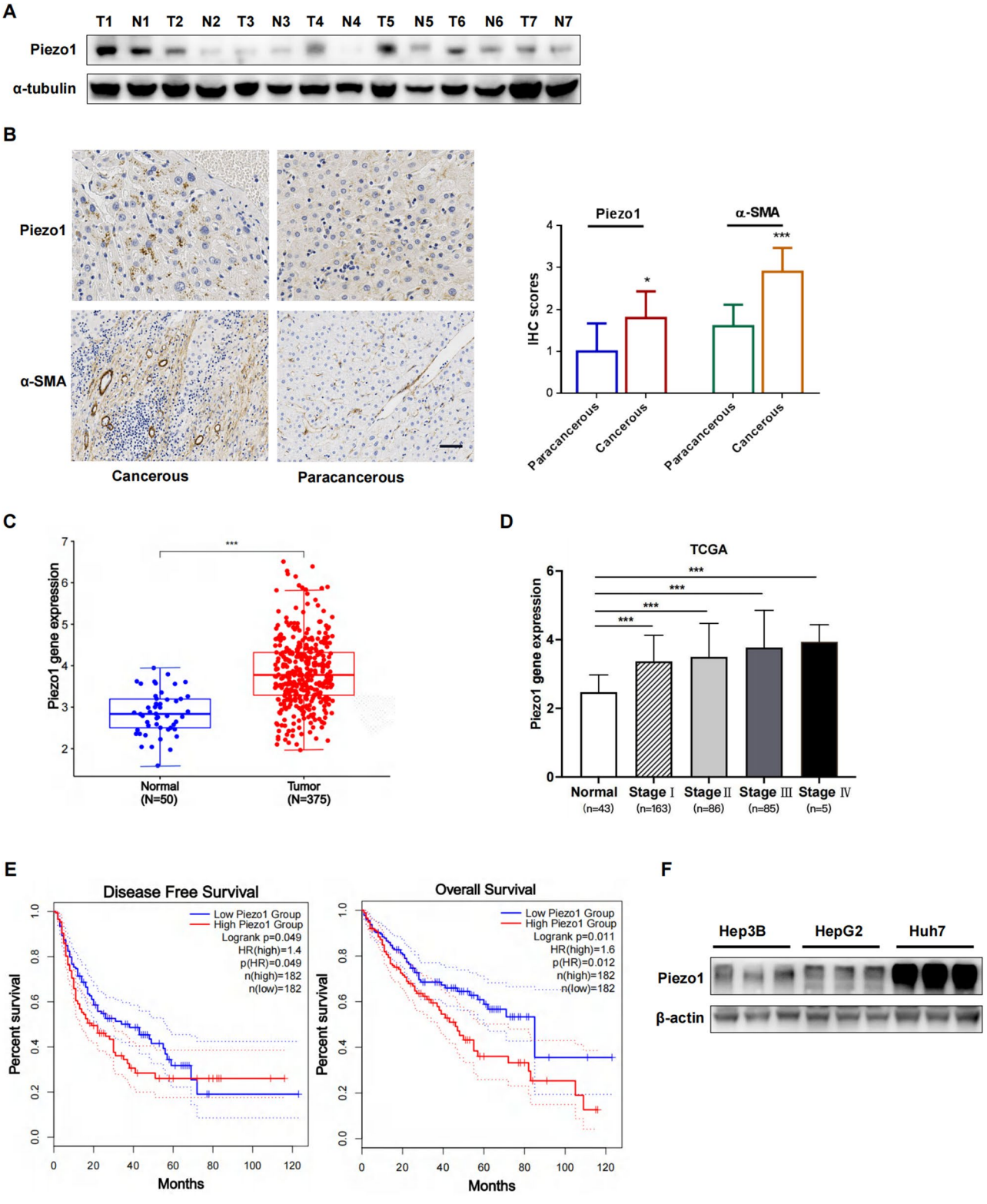

Fig. 1 (See legend on next page.)

(See figure on previous page.)

Fig. 1 Piezo1 was highly expressed in tumor samples of HCC patients and predicted an unfavorable prognosis. (**A**) Representative western blot analysis of Piezo1 protein expressions in cancerous tissues (T) and matched paracancerous tissues (N) derived from HCC patients who underwent radical hepatectomy ($n=7$). (**B**) Representative IHC staining and scores of Piezo1 and α-SMA protein expression in 8 paired cancerous and paracancerous tissues from HCC patients. Scale bar, 50 μm. (**C**) The relative mRNA levels of Piezo1 in normal tissues ($n=50$) and tumor tissues ($n=375$) based on the data retrieved from the HCC TCGA database. (**D**) Piezo1 gene expression across the four stages of HCC as defined by the TNM classification system in the HCC TCGA dataset. (**E**) Kaplan-Meier curves for disease-free survival (DFS) and overall survival (OS) according to higher and lower Piezo1 gene expression (cut-off value = 50%) in HCC patients using the TCGA data. The DFS and OS outcomes were compared using the log-rank test. (**F**) Representative western blot analysis of detecting Piezo1 protein expression signals in Hep3B, HepG2, and Huh7, three HCC cell lines. $^{*}P<0.05$, $^{***}P<0.001$

and those below the median as low expression) using the log-rank test ($P<0.05$) (Fig. 1E). Finally, to investigate the role of Piezo1 in HCC cells, we assessed the protein expression of Piezo1 in Hep3B, HepG2, and Huh7, three HCC cell lines. As shown in Fig. 1F, Piezo1 expression was detected in all three HCC cell lines, with the highest protein levels observed in Huh7 cells.

Modulation of Piezo1 channel activation affected the cellular events of HCC

To explore the Piezo1 function on Huh7 and HepG2 cells, we achieved the Piezo1 channel activation model by using a Piezo1-specific agonist, Yoda1 or Piezo1 siRNAs. Knockdown efficiencies were examined in Huh7 cells transiently transfected with Piezo1 siRNAs (three Piezo1 siRNAs, namely siPiezo1-1#, 2#, 3#) by real-time PCR and western blot analysis, and siPiezo1-3# was selected for subsequent experiments (Fig. S1A-S1C). In order to test the specificity of Piezo1 siRNAs, we further examined whether Piezo2 protein was affected by specific Piezo1-knockdown. The data showed that the signals of Piezo2 protein expression had no changes after Piezo1-knockdown (Fig. S1C).

Next, we choose 1 μM and 10 μM of Yoda1 to examine the specific activities on Piezo1 channel by intracellular calcium influx analysis. Data suggested that at both concentration, fluorescence signals were increased after 0–30 min of Yoda1 assessment and at a high concentration of Yoda1 (10 μM) had a more significant effect on Ca^{2+} influx than low concentration of Yoda1 (1 μM) in Huh7 cells (Fig. S1D). Therefore, we further used 10 μM Yoda1 to explore the Piezo1 function after its channel activation on Huh7 and HepG2 cells. The activation of Yoda1 (10 μM) at various time points in both Huh7 and HepG2 cells, as depicted in Fig. 2A. We noted that the increase in fluorescence intensity immediately detected after 1 min of Yoda1 assessment and peaked around 30 min in Huh7 cells and 1 h in HepG2 cells, followed by gradual declining signals in both cell lines (Fig. 2A). A BrdU assay was conducted to examine the proliferative activities of Huh7 and HepG2 cells after Yoda1 stimulation for 24 h via flow cytometry analysis. A significant increase in fluorescence intensity was observed in Huh7 cells stimulated with Yoda1 compared to control cells by a FlowJo analysis (Fig. 2B). In contrast, the proliferation process was significantly prevented in the Piezo1-knockdown HCC cells treated with Yoda1 (Fig. 2B). This observation was further supported by the Cell Titer-Glo® Luminescent Assay, as in line with previous findings, cell proliferation was markedly elevated in both Huh7 and HepG2 cells treated with Yoda1 compared to controls, and alternatively, the accelerated proliferative activities were blocked in Piezo1-knockdown groups ($P<0.05$) (Fig. 2C). No significant increased cell apoptosis was detected in the 10 μM Yoda1 treatment groups compared to a control group by flow cytometry analysis using Annexin V assay in both Huh7 and HepG2 cells ($P>0.05$) (Fig. S1E). Data collected from the wound healing assay and transwell assay showed that in HCC cells treated with Yoda1 exhibiting a significant enhancement in cell migration and invasion relative to the controls, and these effects were impaired in Piezo1-deficiency groups ($P<0.05$) (Fig. 2D and E). Subsequently, we examined the protein levels of E-cadherin, a well-established epithelial-to-mesenchymal transition (EMT)-related marker, in both Huh7 and HepG2 cell lines treated with Yoda1 compared to controls, and the data revealed that in both cell lines, a significant decrease in E-cadherin protein levels was detected in the Yoda1-stimulated groups, and the invasion and migration were prevented in Piezo1-knockdown groups (Fig. 2F). Finally, to ascertain the effect of activation of Piezo1 on its signaling pathways, we cultured Huh7 cells and stimulated them with 10 μM Yoda1 for varying durations: 0 min, 5 min, 30 min, 1 h, 2 h, and 4 h. The expression of p-ERK1/2, p-AKT, and p-mTOR significantly increased after 5 min of Yoda1 exposure, and the signals gradually declined over time (Fig. 2G). In summary, these findings demonstrated that modulated Piezo1 channels in HCC cells had the following cellular effects including proliferation, migration, invasion and likely mediated these events via PI3K/AKT/mTOR signaling pathways.

Downstream molecular profiling of Piezo1 channel activation by Yoda1 in HCC cells

We conducted a comprehensive transcriptome analysis to further elucidate the potential downstream targets involved in the Piezo1 channel activation. Triplicates from Huh7 cells treated with Yoda1 (10 μM) for 24 h and untreated controls were collected in TRIzol, and then, the six samples were sent to Hangzhou LC Bio Technology Co., Ltd. (China) for RNA-Seq analysis using the

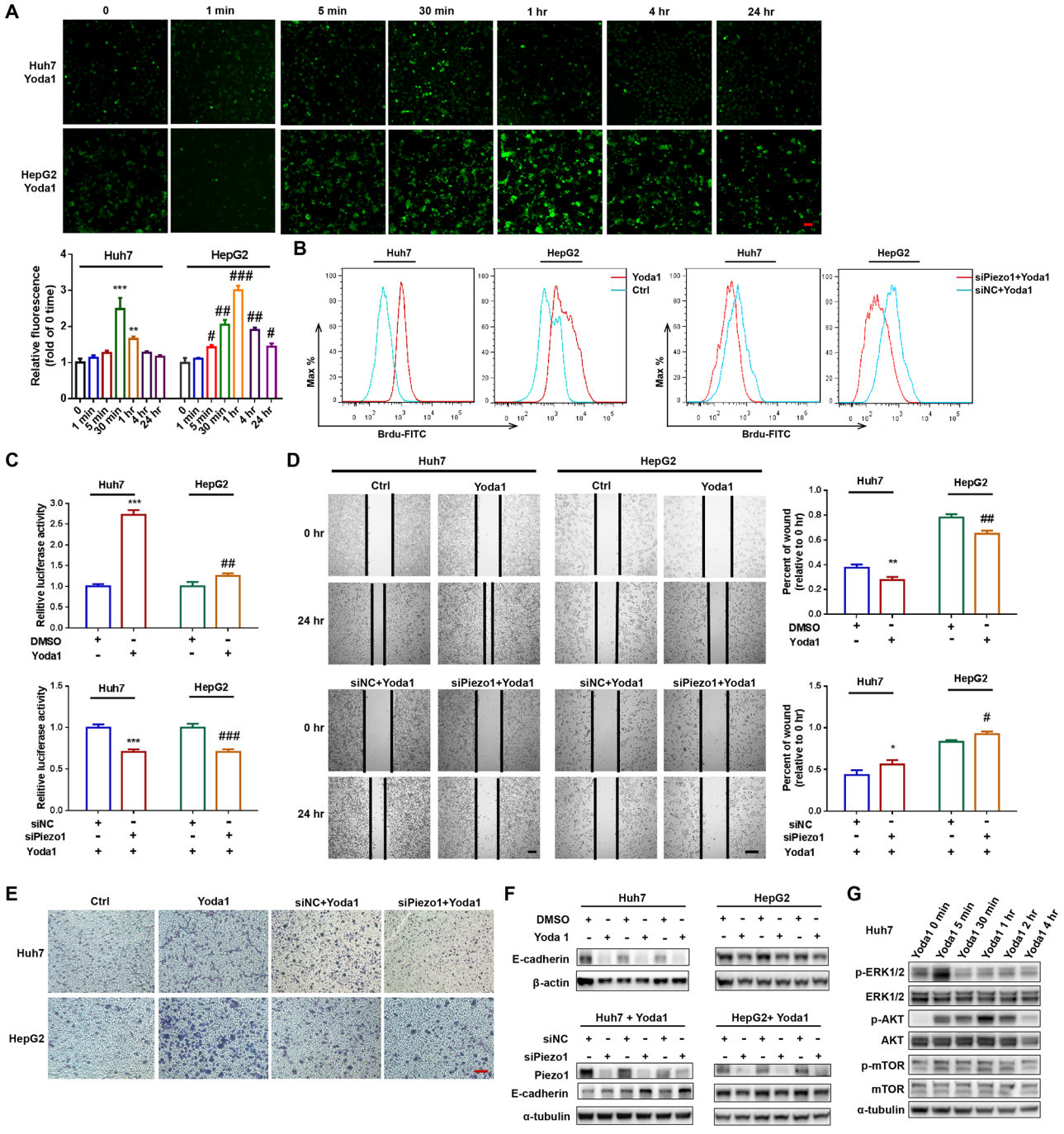

Fig. 2 Modulation of Piezo1 channel activation affected HCC cell proliferation, migration, and invasion. (**A**) Intracellular calcium fluorescence probe (Fluo-4 AM) and relative fluorescence showed the calcium influx into Huh7 and HepG2 cells after treatment with a specific Piezo1 channel agonist, Yoda1, at the dose of 10 μM for 0 min, 5 min, 30 min, 1 h, 4 h and 24 h. Scale bar, 100 μm. (**B**, **C**) The BrdU assay and Cell Titer-Glo® luminescent assay detected cellular proliferative abilities in Huh7 and HepG2 cells after the cells were treated with 10 μM Yoda1 for 24 h, or in Piezo1-knockdown cells treated by 10 μM Yoda1 for 24 h. (**D**) The wound healing assay showed the migration abilities of Huh7 and HepG2 cells. Wound closures were quantified at the bottom. Scale bar, 100 μm. (**E**) The transwell assay showed the invasion abilities of Huh7 and HepG2 cells. (**F**) Western blot analysis showed E-cadherin protein levels in Huh7 and HepG2 cells. (**G**) Western blot detection of p-ERK1/2, ERK1/2, p-AKT, AKT, p-mTOR and mTOR expression in Huh7 cells after treatment with 10 μM Yoda1 for 0 min, 5 min, 30 min, 1 h, 2 h and 4 h. *$P < 0.05$, **$P < 0.01$, ***$P < 0.001$; #$P < 0.05$, ##$P < 0.01$, ###$P < 0.001$

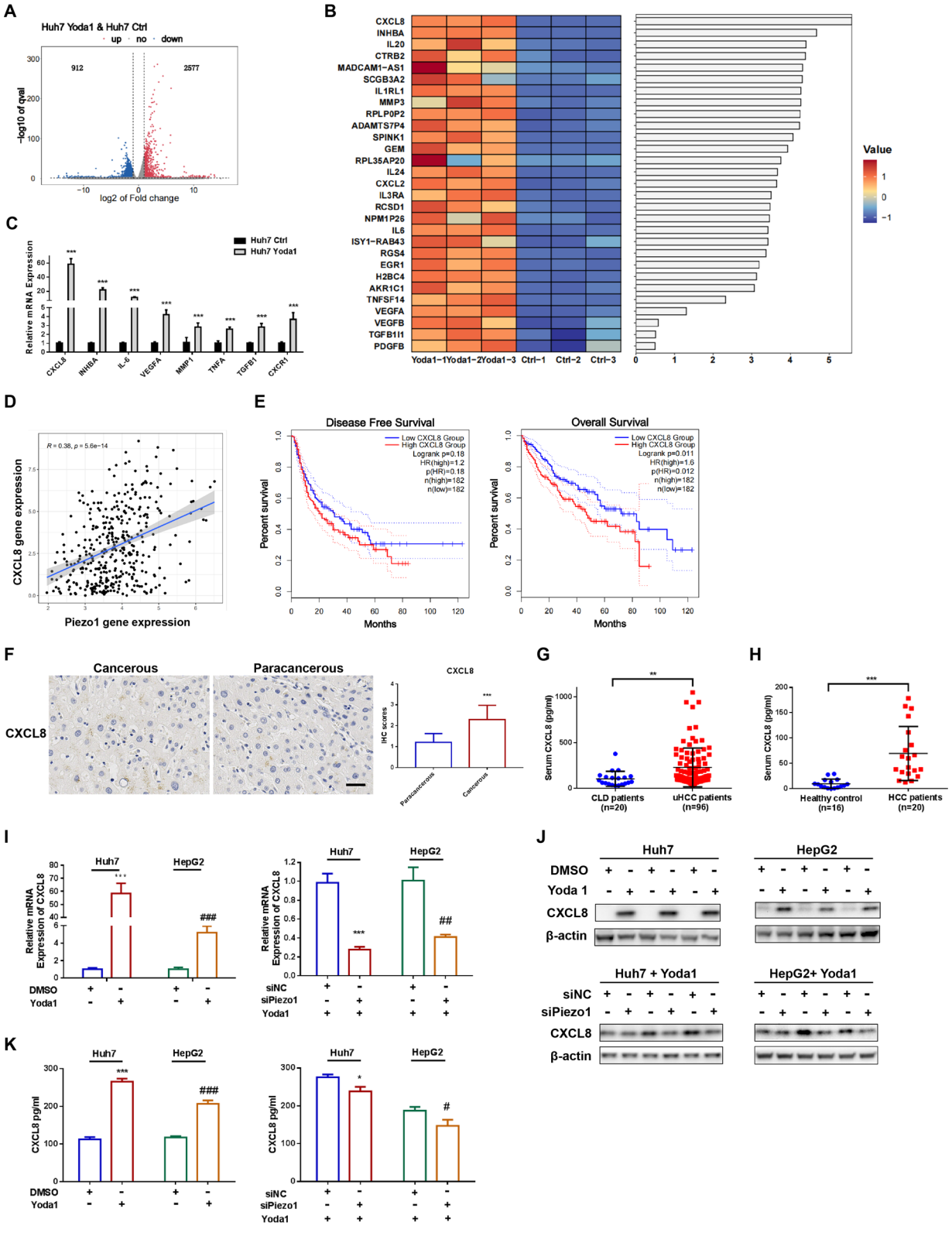

Fig. 3 (See legend on next page.)

(See figure on previous page.)

Fig. 3 Downstream molecular profiling of Piezo1 channel activation by Yoda1 in HCC cells. (**A**) Volcano plot showed the genes significantly affected by 10 μM Yoda1 treatment for 24 h in Huh7 cells compared with control groups, statistically up-regulated (red) and down-regulated (blue) by an RNA-seq analysis. (**B**) Heat map showed the top 29 genes that were positively associated with Piezo1 activation in Huh7 cells by RNA sequencing. (**C**) The representative genes affected by Yoda1 treatment, including *CXCL8*, *INHBA*, *IL-6*, *VEGFA*, *MMP1*, *TNFA*, *TGFB1*, and *CXCR1*, were validated by the real-time PCR experiment. (**D**) A positive correlation between CXCL8 and Piezo1 gene expression was shown in the HCC TCGA database. (**E**) Kaplan-Meier curves for DFS and OS according to the higher and lower mRNA levels of CXCL8 in HCC patients (cut-off value = 50%). (**F**) Representative IHC staining and scores of CXCL8 expression in 8 paired cancerous and paracancerous tissues from HCC patients. Scale bar, 50 μm. (**G**) Scatter plot indicated a difference in serum concentration of CXCL8 between chronic liver disease (CLD, $n = 20$) and treatment-naïve unresectable HCC (uHCC, $n = 96$) patients from a dataset retrieved from GSE261672. (**H**) Serum CXCL8 level was examined by ELISA in healthy controls ($n = 16$) and treatment-naïve HCC patients ($n = 20$). (I) The mRNA levels of *CXCL8* in Huh7 and HepG2 cells. (**J**) Western blot analysis of CXCL8 protein expression in Huh7 and HepG2 cells. (**K**) ELISA analysis of secreted CXCL8 in the medium of Huh7 and HepG2 cells. *$P < 0.05$, **$P < 0.01$, ***$P < 0.001$; #$P < 0.05$, ##$P < 0.01$, ###$P < 0.001$

Illumina Novaseq 6000 platform. After a comprehensive analysis, data revealed 912 up-regulated and 2577 down-regulated genes deferentially expressed between the two groups (Fig. 3A). In the Yoda1-treated group, 3% of genes were significantly increased in intensity, and close to 17% of those genes were enhanced by more than 10-fold (Fig. 3A). Among these genes, a subset of pro-inflammatory cytokines, including CXCL8, INHBA, IL-6, IL-20, IL-24, and CXCL2, were up-regulated with statistical significance ($P < 0.05$) (Fig. 3B). Notably, CXCL8 was among the top list of these cytokines with more than a 40-fold increase (Fig. 3B). Subsequently, we performed real-time PCR experiments to validate these data generated by RNA-seq analysis. The data showed that mRNA levels of *CXCL8*, *INHBA*, *IL-6*, *VEGFA*, *MMP1*, *TNFA*, *TGFB1* and *CXCR1* genes were significantly up-regulated in Yoda1-treatment groups compared to control groups (Fig. 3C). The dose-response relationship of Yoda1-induced CXCL8 gene expression was further examined, showing a 1.8-fold increase at 1 μM and a 50-fold increase at 10 μM in the respective treatment groups ($P < 0.05$) (Fig. S2A). The spearman's correlation analysis revealed a positive correlation in gene expression between Piezo1 and CXCL8 using the HCC TCGA dataset ($R = 0.38$, $P < 0.001$) (Fig. 3D); and further, the Kaplan-Meier survival analysis demonstrated that HCC patients with high mRNA levels of CXCL8 experienced poor OS compared to those with low CXCL8 expression (cut-off value = 50%) ($P = 0.012$), but no significant difference was observed in DFS between the two groups ($P > 0.05$) (Fig. 3E). We continued to use the TCGA data to study the stratified survival analysis on patients categorized by combined Piezo1/CXCL8 expression patterns. The data showed that in the Piezo1 high group with Piezo1 gene expression levels above the median (≥ 50%), the patients were further categorized into CXCL8 high and CXCL8 low groups (cutoff 50%), and the survival outcomes of the groups were examined and compared by log-rank tests. There was no significant difference observed in both groups, with a *P* value> 0.05 (Fig. S2B). Again, in the Piezo1 gene expression levels below the median (< 50%), the overall survival time between the CXCL8 high and low groups has also no difference (Fig. S2C). However, after using a 60%/40% cutoff, the gene expression of Piezo1 in the Piezo1 high expression group, CXCL8 were categorized into high and low (cutoff 60%/40%), and a significant decrease in survival time was observed in CXCL8 higher group ($P < 0.05$) (Fig. S2D). In the Piezo1 low expression group (bottom 40%), a decrease in overall survival time was also been found in the CXCL8 high group (cutoff 60%/40%)($P < 0.05$) (Fig. S2E).

Additionally, the up-regulated expression of CXCL8 protein was recorded in cancerous tissues compared to paracancerous tissues in HCC patients by IHC assays ($P < 0.05$) (Fig. 3F). To further explore the concentration of CXCL8 in the peripheral blood of patients with advanced HCC, protein array data generated from a Luminex assay were downloaded from the GSE261672. After an analysis, results revealed higher serum levels of CXCL8 in 96 treatment-naïve unresectable HCC patients (uHCC) compared to 20 cases of chronic liver disease (CLD) ($P < 0.05$) (Fig. 3G). Consistently, using an ELISA assay, significantly higher CXCL8 (69.6 ± 11.9 pg/mL) was detected in the serum of treatment-naïve HCC patients ($n = 20$) compared to healthy controls ($n = 16$, 9.8 ± 2.29 pg/mL) using samples derived from our medical center ($P < 0.05$) (Fig. 3H). We observed that both mRNA and protein levels of CXCL8 were significantly elevated in the Yoda1-treated groups compared to controls in both Huh7 and HepG2 cells, whereas they were decreased in the Piezo1-knockdown groups ($P < 0.05$) (Fig. 3I and J). The secreted CXCL8 was further examined in the culture supernatant of the HCC cells and Piezo1-depletion cells stimulated with Yoda1 treatment using ELISA. The increased CXCL8 release was also found in the Yoda1-treated groups compared to the controls in both Huh7 and HepG2 cells, and evidently, the secretion of CXCL8 was suppressed in the Piezo1-depletion HCC cells ($P < 0.05$) (Fig. 3K).

Piezo1 channel activation mediated the pro-inflammatory responses via an increase in the release of CXCL8 into the tumor microenvironment

To further confirm the increased expression of CXCL8 was likely to be regulated at transcriptional levels, we performed dual luciferase reporter assays. After successfully

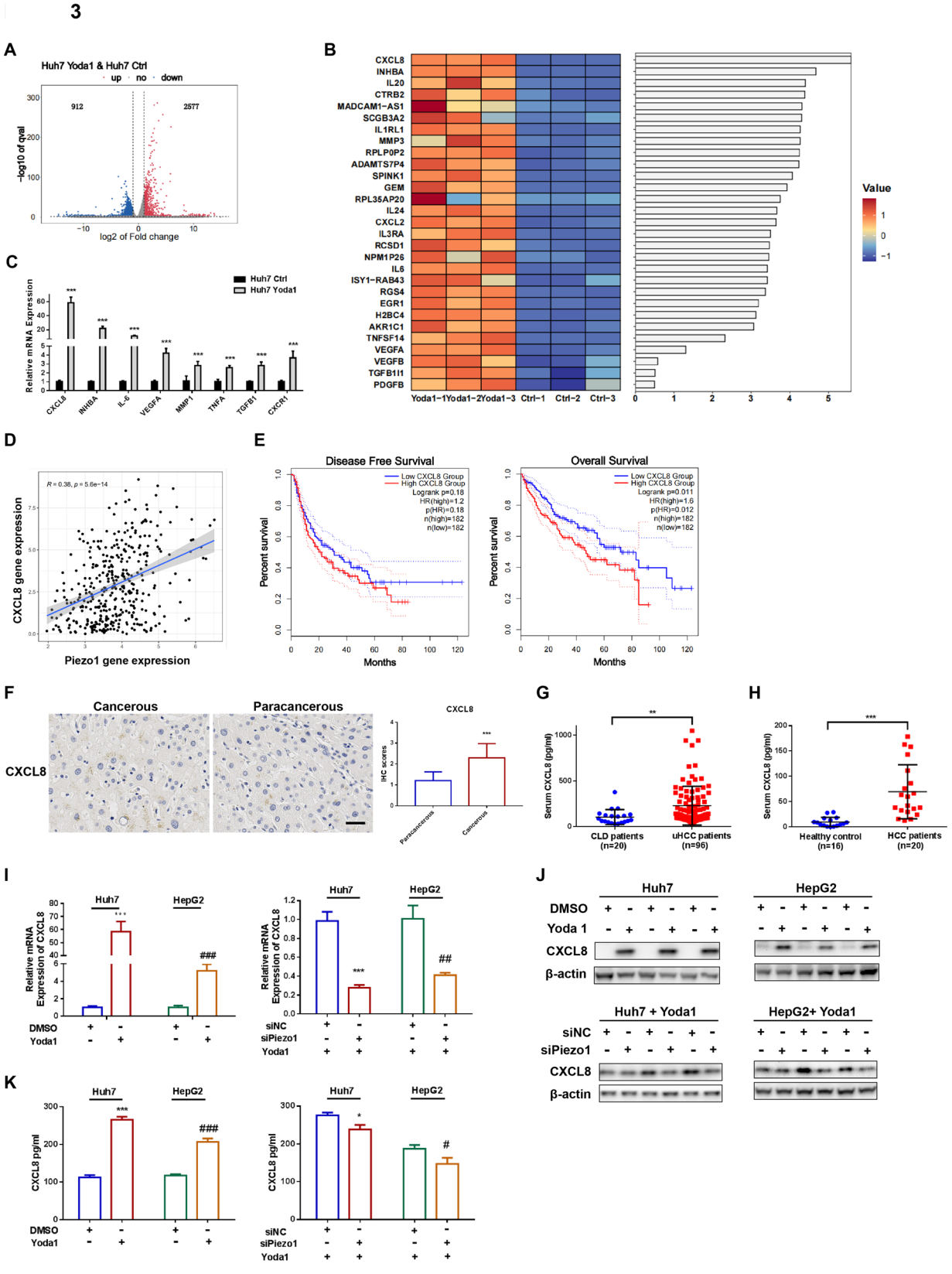

Fig. 4 (See legend on next page.)

(See figure on previous page.)

Fig. 4 Piezo1 channel activation mediated the pro-inflammatory responses via an increase in the release of CXCL8 into the tumor microenvironment. (**A**) Dual luciferase reporter assay recorded the luciferase activity in the Huh7 cells transfected with GPL4-Basic and GPL4-CXCL8 plasmids. (**B**) Using the Huh7 cells transfected with GPL4-Basic and GPL4-CXCL8 plasmids, the luciferase activities were examined in the Huh7 cells pre-treated with 1 μM SCH772984 and 10 μM MK-2206 for 2 h, and then treated with 10 μM Yoda1 for 24 h thereafter. (**C**) Schematic diagram describing the experimental procedure of the PBMC migration assay in vitro. (**D**) PBMC migration assay in the presence of hrCXCL8 (10, 100 and 1000 ng/mL). (**E**) PBMC migration assay in the presence of conditioned medium cultured with or without Huh7 and HepG2 cells exposed to 10 μM Yoda1 for 24 h. (**F**) Tube formation assay using HUVECs cultured with 1% DMSO, or 10 μM Yoda1, or hrCXCL8, or conditioned medium derived from Huh7 treated with 10 μM Yoda1 for 8 h. (**G**) The mRNA levels of *VEGF-A* in Huh7 and HepG2 cells after treatment with 10 μM Yoda1 for 24 h. (**H**) ELISA assay analyzed the release of VEGF protein in the medium of Huh7 and HepG2 cells after treatment with 10 μM Yoda1 for 24 h. *$P < 0.05$, ***$P < 0.001$; #$P < 0.05$, ###$P < 0.001$

generating the constructs GPL4-Basic and GPL4-CXCL8, they were transiently transfected in the Huh7 cells followed by treatment with Yoda1 for 24 h, and then the luciferase activity was measured. Figure 4A showed that the luciferase activity of HCC cells transfected with GPL4-CXCL8 constructs was significantly higher after Yoda1 simulation compared to GPL4-Basic, with more than a 50-fold increase ($P < 0.05$). Furthermore, the highly selective inhibitors SCH772984 for ERK1/2 and MK-2206 for AKT were employed to assess whether the Piezo1/MEK/ERK or Piezo1/PIK3/AKT signaling pathways were involved in modulating the promoter region of CXCL8, thereby enhancing its transcriptional expression in HCC cells. The dual luciferase assay revealed a modest yet significant reduction in luminescence signals in Huh7 cells that were transiently transfected with GPL4-Basic and GPL4-CXCL8 plasmids followed by pretreated with SCH772984 (ERK1/2i) or MK-2206 (AKTi) for 2 h and then exposed to 10 μM Yoda1 for 24 h thereafter ($P < 0.05$) (Fig. 4B). This finding supported the involvement of both MEK/ERK and PIK3CA/AKT signaling cascades in the induction of CXCL8 gene expression subsequent to Piezo1 ion channel opening. To further investigate whether the secreted CXCL8 followed by Piezo1 activation in HCC mediated the recruitment of immune cells into the tumor microenvironment, an immune cell trafficking experiment was conducted in a co-culture system. PBMCs were isolated from six healthy donors and cultured with conditioned medium (CM) or hrCXCL8 at concentrations of 10 ng/mL, 100 ng/mL, and 1000 ng/mL (Fig. 4C). We noted a concentration-dependent increase in the number of PBMC migration upon the addition of hrCXCL8, peaking at 1000 ng/mL ($P < 0.05$) (Fig. 4D). Similarly, the number of PBMC migration was significantly elevated when cultured with CM derived from Yoda1-treated HCC cells ($P < 0.05$), but with no significant difference observed upon supplementation to DMSO or Yoda1 (10 μM) alone as controls ($P > 0.05$) (Fig. 4E). This finding rules out the possibility of the effects PMBC migration which may be affected by the Yoda1 remaining in the conditioned medium rather than CXCL8 released by HCC cells. As depicted in Fig. 4F, the CM of Huh7 cells from the Yoda1 treatment group and the hrCXCL8 group (100 ng/mL) promoted increased capillary network formation compared to control groups, suggesting the increased CXCL8 release by HCC cells after Piezo1 channel opening actively contributed to angiogenesis in the TME of HCC. We observed that the mRNA expression of *VEGFA* was significantly elevated in the Yoda1-treated groups compared to controls in both Huh7 and HepG2 cells ($P < 0.05$) (Fig. 4G). The secreted VEGF was further examined in the culture supernatant of the HCC cells stimulated with Yoda1 treatment using ELISA. The increased VEGF release was also found in the Yoda1-treated groups compared to the controls in both Huh7 and HepG2 cells ($P < 0.05$) (Fig. 4H). In summary, these findings suggested that the activation of the Piezo1 signaling pathway was crucial for the release of CXCL8 into the TME in HCC.

Piezo1 channel activation modulated mitochondrial stress via regulating MTHFD2, a metabolic checkpoint enzyme

After a KEGG pathway enrichment analysis, the genes regulated by the Yoda1-treated Huh7 cells were highly clustered within the metabolic pathways (Fig. 5A). To further confirm Piezo1 channel activation induced mitochondrial metabolic function, ROS was measured by a non-fluorescent probe of DCFH-DA, and mitochondrial membrane potential was evaluated by a TMRM probe. Compared to the control group, increased ROS and TMRM were observed in Yoda1-treated group for 24 h in Huh7 cells (Fig. 5B and C). From our previous published work, we found that MTHFD2, a bifunctional enzyme involved in one-carbon metabolic pathways, was associated with oxidative stress of mitochondria [20]. Interestingly, we found that the gene expression of Piezo1 was positively correlated with MTHFD2 using HCC samples from the TCGA database. ($P < 0.05$) (Fig. 5D). We also used the TCGA data to study the stratified survival analysis on patients who were further categorized by combined MTHFD2/Piezo1 expression patterns. In the MTHFD2 high expression group, an unfavorable survival outcome was observed in the Piezo1 high expression group, and the difference was statistically significant (cutoff value 50%/50%, $P < 0.05$) (Fig. S2F). Alternatively, in the MTHFD2 low expression group, no difference in OS was observed between the Piezo1 high and low expression groups ($P > 0.05$) (Fig. S2G). The regulation of MTHFD2 expression were investigated after Piezo1 channel activation by Yoda1 treatment in Huh7 cells or

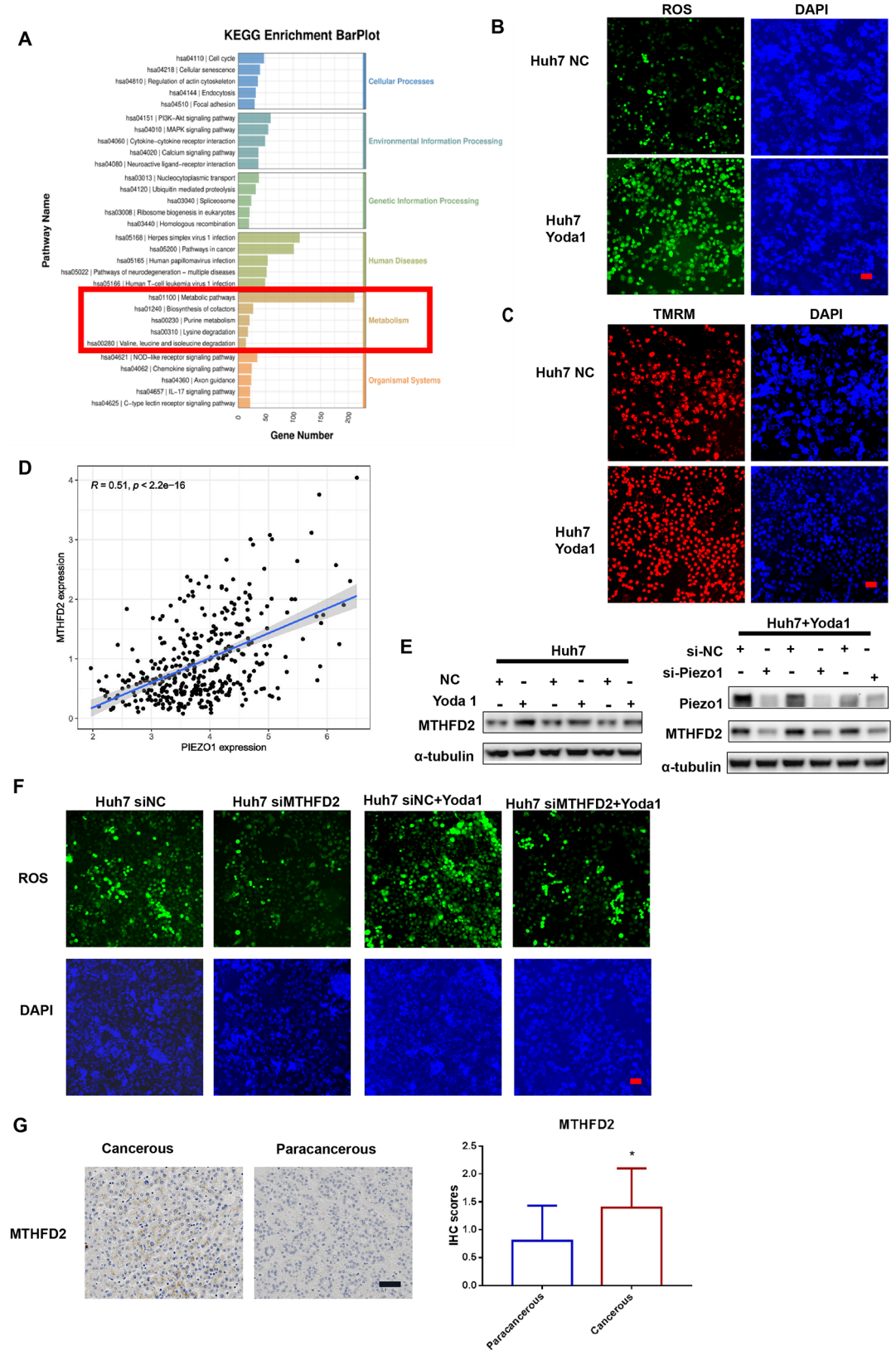

Fig. 5 (See legend on next page.)

(See figure on previous page.)

Fig. 5 Piezo1 channel activation influenced the mitochondrial dynamics via mitochondrial one-carbon metabolic enzyme (MTHFD2). (**A**) KEEG analysis showed the signaling pathways associating with Piezo1 channel activation by Yoda1 in Huh7 cells compared with control groups. (**B**, **C**) Intracellular ROS assay (a non-fluorescent probe of DCFH-DA) and mitochondrial membrane potential (TMRM probe) showed the fluorescent signals of ROS and TMRM increased in Huh7 cells after treatment with 10 μM Yoda1 for 24 h. Scale bar, 100 μm. (**D**) A positive correlation between MTHFD2 and Piezo1 gene expression in the HCC TCGA database. (**E**) Western blot analysis of MTHFD2 protein expression in Huh7 cells and Piezo1-depleted Huh7 cells treated with 10 μM Yoda1 for 24 h compared to controls, respectively. (**F**) The fluorescent signals of ROS detected in MTHFD2-depleted Huh7 cells treated with or without 10 μM Yoda1 for 24 h. Scale bar, 100 μm. (**G**) Representative IHC staining and scores of MTHFD2 protein expression in 8 paired cancerous and paracancerous tissues from HCC patients. Scale bar, 50 μm. *$P < 0.05$

in the cells with siRNA Pieoz1 knockdown. As shown in Fig. 5E, the expression of MTHFD2 protein was significantly increased in the Yoda1 treatment group, and alternatively, reduced in Piezo1-knockdown HCC cells. Not surprisingly, ROS production was significantly down-regulated in the MTHFD2-depleted Huh7 cells compared to the controls (Fig. 5F). A significant decrease in the fluorescent signals of ROS was also observed in MTHFD2-depleted Huh7 cells after they were stimulated by Yoda1 for 24 h compared to the controls (Fig. 5F). In the subsequent study, we further studied the expression of MTHFD2 protein in the tumor tissues of HCC patients. The results showed that expression of MTHFD2 protein was elevated in the cancerous tissues compared to adjacent paracancerous tissues from HCC patients by an IHC assay ($P < 0.05$) (Fig. 5G).

Piezo1 knockdown inhibited tumor growth in vivo

According to our earlier findings, we conducted further research to investigate the impact of Piezo1 deficiency on tumor growth in vivo. Initially, cell fluorescence and western blot analyses confirmed Piezo1-knockdown efficiency in Huh7 cells (Fig. S3A, 6A). In order to test the specificity of shRNA Piezo1, we also conducted western blot assay to examine whether Piezo2 protein was affected by specific Piezo1 shRNA knockdown. Data showed that Piezo2 protein expression was not affected by the specific Piezo1 shRNA knockdown in Huh7 cells (Fig. 6A). We then established a tumor formation model by subcutaneously injecting Huh7 cells, which had been transfected with either shVec or shPiezo1, into nude mice. After 10 days, when tumors became visible, we monitored the development of tumor nodules in these mice (Fig. 6B). As depicted in Fig. 6C and D, tumors in the shPiezo1 group exhibited slower growth and smaller size of tumor nodules compared to those in the shVec group ($P < 0.05$). Finally, mice were sacrificed by cervical dislocation for tumor sample harvesting for HE staining as well as IHC for the protein expressions of Piezo1, MTHFD2, CXCL8, VEGFα and Ki-67. The protein levels of Piezo1, MTHFD2 and VEGFα were significantly lower in the shPiezo1 group compared to the shNC group, and the tumor cell proliferation rate, as indicated by Ki-67 staining, was also decreased in this group ($P < 0.05$) (Fig. 6E and F). However, CXCL8 protein signals were weak both in the shPiezo1 and shNC groups without statistical differences ($P > 0.05$) (Fig. 6E and F). In summary, the suppression of Piezo1 expression in HCC cells significantly affected tumor proliferation and angiogenesis in a tumor-bearing mouse model.

Blocking Piezo1 channel together with oxaliplatin displayed synergistic anti-tumor effects in HCC

Oxaliplatin-based chemotherapy became a standard treatment strategy for advanced HCC. The IC50 value of oxaliplatin was examined in a broad range of doses from 0.02 to 25 μM for 3 days, and 2.47 μM was determined to be the IC50 value (Fig. 7A). To evaluate whether blocking the Piezo1 channel improved the anti-tumor sensitivities of oxaliplatin, we used the previously identified Piezo1 channel inhibitors, including GsMTx4 and arachidonic acid (AA) [16]. Compared to oxaliplatin alone, oxaliplatin combined with GsMTx4 or AA suppressed Huh7 cell proliferation in a concentration-dependent manner (0.1 to 20 μM) ($P < 0.05$) (Fig. 7B and C). Time-course assay showed that GsMTx4 and AA promoted the anti-tumor effect of oxaliplatin in a time-dependent manner (0–4 day) ($P < 0.05$) (Fig. 7D). At the concentration of GsMTx4 5 μM and arachidonic acid 10 μM, Yoda1 induced Ca^{2+} influx was completely blocked in Huh7 cells (Fig. 7E). Finally, compared to the oxaliplatin group alone, both GsMTx4 (5 μM) and AA (10 μM) combined with oxaliplatin groups had a significant decrease in cell viability, indicating synergistic anti-tumor effects of Piezo1 antagonists together with oxaliplatin in HCC ($P < 0.05$) (Fig. 7F).

Discussion

It has long been established that chronic liver diseases, such as hepatic viral infection, excessive alcohol consumption, and NAFLD, can result in liver cirrhosis, subsequently elevating the risk of HCC [5]. In a cirrhosis state, multiple cell types, including hepatocytes, hepatic stellate cells (HSCs), sinusoidal endothelial cells (SECs), and Kupffer cells (KCs), contribute to the progress of liver fibrosis, a condition characterized by the accumulation of extracellular matrix (ECM) and the formation of scar tissues that replace the normal liver architecture [21]. The expedited matrix deposition in the tumor environment may be responsible for the increased stiffness of tumor tissues, which further promotes tumor progression [22].

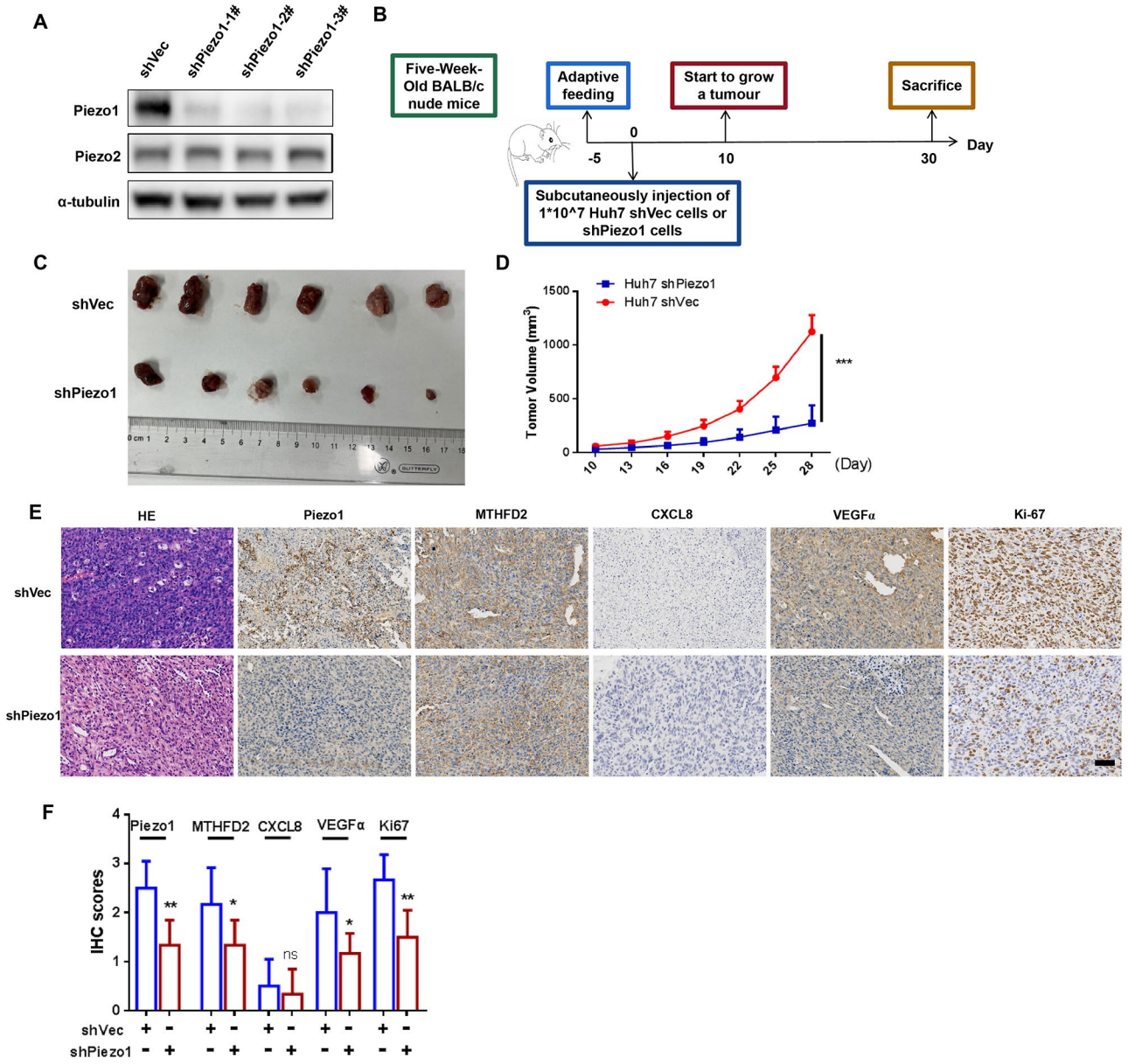

Fig. 6 Depletion of Piezo1 protein in the HCC cells inhibited the tumor growth and angiogenesis in vivo. (**A**) Western blot assay showed the knockdown efficiency of Piezo1 in Huh7 cells transfected by Piezo1 shRNA lentiviral vectors. (**B**) Schematic diagram showing the experimental procedures in BALB/c nude mice subcutaneously injected with Piezo1-depleted Huh7 cells ($n=6$). (**C**) Representative images of tumor volumes in mice treated with shVec and shPiezo1. (**D**) Tumor growth curve of shVec- and shPiezo1-treated HCC tumors in mice. (**E**) Representative HE staining and IHC staining and scores of Piezo1, MTHFD2, CXCL8, VEGFα and Ki67 protein expressions in the recent tumor tissues of mice treated with shVec and shPiezo1. Scale bar, 50 μm. $^{*}P<0.05$, $^{**}P<0.01$, $^{***}P<0.001$

In the present study, we revealed a significant up-regulation of Piezo1 expression in cancerous tissues compared to adjacent non-cancerous tissues from HCC patients. Bioinformatics studies using HCC TCGA data showed that the higher mRNA levels of Piezo1 in the tumor tissues are associated with unfavorable DFS and OS. These findings were consistent with prior studies, reporting that Piezo1 was up-regulated in a multitude of malignancies, such as oral squamous cell carcinoma [23], gliomas [24], colorectal [25], gastric [26], bladder [27], prostate [28], and breast cancers [29]. However, it is noteworthy that this trend was not universally observed, as in a study of non-small-cell lung cancer (NSCLC), where low levels of Piezo1 implicated in facilitating cancer cell migration and growth, thereby leading to an unfavorable prognosis in patients with NSCLC who exhibited low expression of Piezo1 [30].

We further validated that an enhanced influx of intracellular Ca^{2+} followed by the activation of the Piezo1 channel, and this biological activity augmented

Figure 7

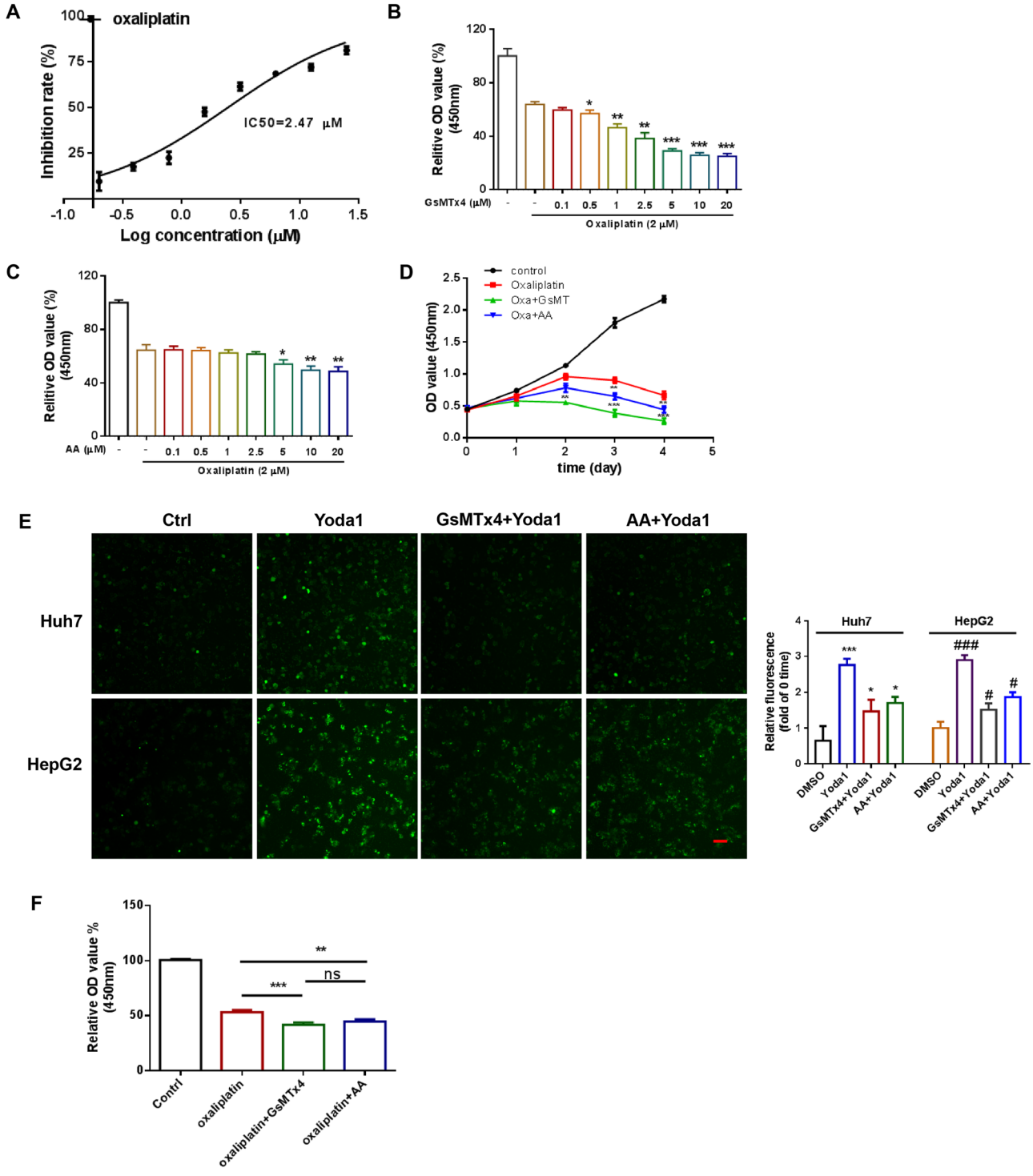

Fig. 7 Blocking Piezo1 channels by its antagonists improved anti-tumor sensitivities induced by oxaliplatin in HCC. (**A**) The IC50 of oxaliplatin was valued in Huh7 cells for 3 days of exposure. (**B**, **C**) Huh7 cells were treated with oxaliplatin (2 μM), oxaliplatin combined with various concentrations of GsMTx4 (**B**) or AA (**C**) for 3 days. Cell viability was detected by a CCK-8 assay. (**D**) Huh7 cells were treated with oxaliplatin (2 μM), oxaliplatin combined with GsMTx4 (5 μM) or AA (10 μM) for the indicated days. Cell viability was detected each day by a CCK-8 assay. (**E**) Huh7 cells were pretreated with GsMTx4 (5 μM) or AA (10 μM) for 2 h and then exposed to Yoda1 (10 μM) for 30 min. Intracellular calcium influx was observed using a Fluo-4 Calcium Assay Kit. (**F**) Huh7 cells were treated with oxaliplatin (2 μM), oxaliplatin combined with GsMTx4 (5 μM) or AA (10 μM) for 3 days. Cell viability was detected by a CCK-8 assay. **P* < 0.05, ***P* < 0.01, *** *P* < 0.001; #*P* < 0.05, ###*P* < 0.001

downstream cascades by metabolic reprogramming and inflammatory responses via promoting mitochondrial oxidative stresses, a range of cellular events including cell proliferation, migration and invasion, EMT, as well as cytokine release. We noted that Yoda1 immediately induced Ca^{2+} influx but delayed peaks (30 min–1 h) in our study. This observation appears to be unusual as ion channel activation typically causes immediate calcium influx followed by rapid desensitization. We considered that there may present discrepancy in the effective Yoda1 induced Ca^{2+} influx in different cell types due to the unique sensitivity to Yoda1. In addition, other more sensitive methodologies, such as a patch clamp experiment, may be required for earlier and more accurate detection of Ca^{2+} influx, which can partially overcome this limitation.

Data generated a KEGG pathway enrichment analysis after an RNAseq analysis in HCC cells with piezo1 activation, showing that cells treated by Yoda1 were highly clustered within PI3K-AKT signaling, purine metabolism and metabolic pathways etc. Induced ROS were detected in Piezo1-activated liver cancer cells, and this effect appeared to be mediated by its downstream target, MTHFD2. ROS induces rapid depolarization of inner mitochondrial membrane potential and participates in a variety of pathogenic processes, including inflammation, aging, immune response, and signal transduction [31]. MTHFD2, an essential enzyme in this one-carbon metabolic pathway, which is up-regulated in various cancer cells including HCC, plays important roles in cancer cells growth and is responsible for the poor prognosis of many cancer types [32–34]. In our previous published work, we showed that MTHFD2 had roles in metabolic activities involving mitochondrial dynamic function and served as a novel therapeutic candidate in LUAD [20]. Several other studies showed that the presence of MTHFD2 in mitochondria maintained the integrity of the mitochondrial respiratory chain and prevented mitochondrial dysfunction [35]. For instance, MTHFD2 depletion mediated mitochondrial dysfunction by decreasing UQCEC2 gene expression [36]. In our present study, we observed that Yoda1-induced MTHFD2 protein expression diminished in Piezo1-deleted Huh7 cells, suggesting that MTHFD2 is likely to be the mitochondrial core enzyme regulated by the stimulation of the Piezo1 channel and plays its metabolic activities in followup. However, the mechanistic connection between Piezo1 and MTHFD2 needs to be further clarified. It will be extremely important to answer whether the effect of Yoda1 induced enzyme activity of MTHFD2 is a straightforward or indirect reaction in the future study.

A group of cytokines had been identified as the downstream molecules affected by Piezo1 activation. Among them, CXCL8 stood out as the most significantly up-regulated protein. Alternatively, impairing the release of CXCL8 followed by knocking down Piezo1 protein confirmed that the activation of Piezo1 channels in cancer cells triggers signal pathways that were responsible for the secretion of CXCL8 into the tumor environment. CXCL8, also referred to as IL-8, is a chemokine of the CXC family that has been established to contribute to cell migration and EMT events [37]. CXCL8 primarily exerts its biological functions through the binding of CXCR1 and CXCR2, two G protein-coupled receptors that are ubiquitously expressed on granulocytes, monocytes, endothelial, and cancer cells [38, 39].

In our study, we also discovered a positive correlation between CXCL8 and Piezo1 in the gene expression of the HCC TCGA datasets. CXCL8 gene and protein expression were also up-regulated in the HCC tissues and correlated to poor OS. Furthermore, higher serum levels of CXCL8 were detected in treatment-naive advanced HCC patients compared to healthy controls, which was corroborated by a GEO dataset (GSE 261672), a protein array encompassing a spectrum of cytokines generated through Luminex assay [15].

Previous studies have well-established that enhanced concentrations of circulating CXCL8 correlate strongly with advanced stages of tumors and unfavorable prognosis for multiple tumor types [38]. In a recent large-scale retrospective analysis, 1,344 patients with advanced cancers were recruited and the study revealed that patients with elevated baseline serum CXCL8 levels exhibited unfavorable clinical outcomes followed by treatment with PD-1 immune-checkpoint inhibitors, suggesting that higher serum CXCL8 level was an independent biomarker in the context of immunotherapy [40]. Our findings indicated that liver cancer cells may serve as the primary source of CXCL8 production within the fibrotic microenvironment of HCC. Our study also demonstrated that CXCL8 might be a major soluble cytokine involved in circulating immune cell trafficking and tumor angiogenesis after Piezo1 channel activation. Additionally, our animal studies reinforced this observation, as the shRNA Piezo1 protein knockdown cell line showed impairment of both tumorigenesis and angiogenesis in nude mice.

The activation of ERK1/2 and AKT signal pathways by the Piezo1-induced signaling cascades was likely leading to the transcriptional up-regulation of CXCL8 in liver cancer cells, as using specific ERK1/2 and AKT inhibitors suppressed CXCL8 expression at a transcriptional level in the liver cancer cells, as evidenced by a dual luciferase reporter assay. The Ras/MEK/ERK pathway, also known as the Ras/mitogen-activated protein kinase (MAPK) cascade, is a signaling pathway that plays a crucial role in the regulation of cell growth, differentiation, and survival [41]. The dysregulation of the PI3K/Akt pathway integrates a number of substrates, including mTOR,

promoting cancer cell proliferation and metastasis [42]. Our findings suggest that the presence of the Piezo1-ERK1/2-CXCL8 and Piezo1/AKT/CXCL8 axis in HCC and the inhibition of Piezo1 activity appear to impede CXCL8 secretion, and thereby Piezo1 may serve as a novel therapeutic target for HCC.

The treatment options for advanced HCC include systemic chemotherapy. Among the regimens for HCC, oxaliplatin is commonly used as the first-line chemotherapeutic drug [43]. However, decreased response to oxaliplatin occurred in the subsequent drug administration due to drug resistance. Therefore, to address this important question, the inhibition of Piezo1 function by a chemical compound or an antagonist was explored to identify the improvement of anti-tumor sensitivities induced by oxaliplatin in HCC. Indeed, increased anti-tumor efficacy induced by GsMTx4 as well as by AA, an essential polyunsaturated fatty acid, was observed in an HCC cell line, indicating that targeting Piezo1 provided therapeutic advantages in the treatment of HCC. Moreover, we further showed the synergistic anti-tumor effects of GsMTx4 or AA together with oxaliplatin in HCC cells. GsMTx4, a peptide from spider venom, has been well established as a gating modifier used to block the activities of Piezo1 channel [44]. In addition to Piezo1, GsMTx4 is able to block other mechanosensitive ion channels (MSCs) including Piezo2 and TRP family members, suggesting it exhibits non-specific inhibitory effects in broader contexts [16]. AA is a polyunsaturated fatty acid known for being involved in numerous biological effects, such as cell proliferation and metabolism [45, 46]. Recently, AA has been proved to serve as a blocker for enhancing inactivation kinetics of the Piezo1 channel [47]. It is necessary to clarify that both antagonists used in our study are non-specific for the Piezo1 channel. Indeed, there is still a lack of specific inhibitors targeting Piezo1 to date. Therefore, exploring novel chemical compounds specifically against this mechanosensitive ion channel remains to be a priority. Nevertheless, our results provided strong evidence that targeting the Piezo1 pathway is a promising strategy for the treatment of HCC.

Limitation of the study: firstly, we only conducted in vitro experiments testing the Piezo1 antagonists on the inhibition of the activity of liver cancer cells and lack of further animal validation. Secondly, it may not fully recapitulate the immune microenvironment in the tumor tissue by only using immunodeficient nude mice. Therefore, other animal models, such as chemical induction models of HCC, particularly the carbon tetrachloride (CCl_4) induced liver cancer model, will provide an extra connection between Piezo1 axis in liver cancer cells and tumor immune microenvironment. Finally, other humanized experimental models, such as human organoid or patient-derived xenograft models, may provide more preclinically relevant validation on the anti-tumor effects of targeting Piezo1.

Taken together, our results demonstrate the present linkage of metabolic reprogramming and pro-inflammatory responses after Piezo1 activation in HCC. Targeting Piezo1 appears to be a novel therapeutic strategy improving the treatment efficacy in HCC.

Supplementary Information

The online version contains supplementary material available at https://doi.org/10.1186/s12964-025-02289-7.

Supplementary Material 1: Figure S1: (A) Western blot assay showed the knockdown efficiency of Piezo1 in Huh7 cells transfected by three Piezo1 siRNA. (B) The Piezo1 gene in Huh7 and HepG2 cells transfected by Piezo1 siRNA was validated by the real-time PCR experiment. (C) Western blot assay showed Piezo1 and Piezo2 in Huh7 and HepG2 cells transfected by Piezo1 siRNA. (D) Intracellular calcium fluorescence probe (Fluo-4 AM) used to detect the calcium influx into Huh7 after treatment with Yoda1(1 μM and 10 μM) for 0 min, 5 min, 30min, 1 hr, 4 hr and 24 hr. Scale bar, 100 μm. (E) The Annexin V assay used to detect apoptosis in Huh7 and HepG2 cells treated with 10 μM Yoda1 for 24 hr.

Supplementary Material 2: Figure S2: (A) The CXCL8 gene expression in Huh7 and HepG2 cells treated with 1 μM and 10 μM Yoda1 for 24 hr by the real-time PCR experiment. (B, C) Kaplan-Meier curves for survival probability according to higher and lower CXCL8 gene expression in the Piezo1 high group and low group with Piezo1 gene expression levels (cutoff value = 50%) in HCC patients using the TCGA data. The survival probability outcomes were compared using the log-rank test. (D, E) Kaplan-Meier curves for survival probability according to higher and lower CXCL8 gene expression in the Piezo1 high group and low group with Piezo1 gene expression levels (cutoff value = 60%/40%) in HCC patients using the TCGA data. The survival probability outcomes were compared using the log-rank test. (F, G) Kaplan-Meier curves for survival probability according to higher and lower Piezo1 gene expression in the MTHFD2 high group and low group with MTHFD2 gene expression levels (cutoff value = 50%) in HCC patients using the TCGA data. The survival probability outcomes were compared using the log-rank test.

Supplementary Material 3: Figure S3: (A) Cell fluorescence density showed Piezo1-knockdown efficiency in Huh7 cells.

Acknowledgements

This work was supported by Science and Technology Bureau of Jiaxing (grant no 2024AY10008, 2023AY11032 and 2025CGZ054).

Author contributions

J.M. and Y.B. contributed the majority study design and drafted the manuscript. Y.Z., C.C. and Y.W. collected the human samplesperformed PCR experiments and clinical bioinformatic analyses. J.M. and Y.B. designed all the experiments, Y.Z., W.Z., S.W., L.Z., and J.W. performed majority in vitro experiments and analyzed the corresponding data. J.M., J.W., Y.Z., and W.Z., performed animal experiments. X.W., and C.C. provided human HCC samples. J.M., J.W. and Y.B. supervised the analysis of the data. J.M. and Y.B. supervised the study and revised the drafted manuscript. All authors contributed to data interpretation, discussion of results, and commented on the manuscript.

Data availability

No datasets were generated or analysed during the current study.

Declarations

Competing interests

The authors declare no competing interests.

Author details
[1]The Key Laboratory, The Second Affiliated Hospital of Jiaxing University, 1518 Huancheng North Road, Jiaxing, Zhejiang 314000, China
[2]Department of Oncology, The Second Affiliated Hospital of Jiaxing University, Jiaxing, Zhejiang, China
[3]Department of Hepatobiliary Surgery, The Second Affiliated Hospital of Jiaxing University, Jiaxing, Zhejiang, China
[4]The Key Laboratory, Department of Oncology, The Second Affiliated Hospital of Jiaxing University, 1518 Huanchen North Road, Jiaxing, Zhejiang 314000, China

Received: 14 February 2025 / Accepted: 4 June 2025
Published online: 13 June 2025

References

1. Llovet JM, Zucman-Rossi J, Pikarsky E, et al. Hepatocellular carcinoma[J]. Nat Rev Dis Primers. 2016;2:16018. https://doi.org/10.1038/nrdp.2016.18.
2. Sung H, Ferlay J, Siegel RL, et al. Global Cancer statistics 2020: GLOBOCAN estimates of incidence and mortality worldwide for 36 cancers in 185 Countries[J]. CA Cancer J Clin. 2021;71(3):209–49. https://doi.org/10.3322/caac.21660.
3. Mcglynn KA, Petrick JL, El-Serag HB. Epidemiology of hepatocellular Carcinoma[J]. Hepatology. 2021;73(Suppl 1):4–13. https://doi.org/10.1002/hep.31288.
4. Yang X, Li Q, Liu W, et al. Mesenchymal stromal cells in hepatic fibrosis/cirrhosis: from pathogenesis to treatment[J]. Cell Mol Immunol. 2023;20(6):583–99. https://doi.org/10.1038/s41423-023-00983-5.
5. Hammerich L, Tacke F. Hepatic inflammatory responses in liver fibrosis[J]. Nat Rev Gastroenterol Hepatol. 2023;20(10):633–46. https://doi.org/10.1038/s41575-023-00807-x.
6. Cheng D, Chai J, Wang H, et al. Hepatic macrophages: key players in the development and progression of liver fibrosis[J]. Liver Int. 2021;41(10):2279–94. https://doi.org/10.1111/liv.14940.
7. Affo S, Filliol A, Gores GJ, et al. Fibroblasts in liver cancer: functions and therapeutic translation[J]. Lancet Gastroenterol Hepatol. 2023;8(8):748–59. https://doi.org/10.1016/S2468-1253(23)00111-5.
8. Liu H, Hu J, Zheng Q, et al. Piezo1 channels as force sensors in mechanical force-Related chronic Inflammation[J]. Front Immunol. 2022;13:816149. https://doi.org/10.3389/fimmu.2022.816149.
9. Kang N. Mechanotransduction in liver Diseases[J]. Semin Liver Dis. 2020;40(1):84–90. https://doi.org/10.1055/s-0039-3399502.
10. Coste B, Mathur J, Schmidt M, et al. Piezo1 and Piezo2 are essential components of distinct mechanically activated cation channels[J]. Science. 2010;330(6000):55–60. https://doi.org/10.1126/science.1193270.
11. Atcha H, Jairaman A, Holt JR, et al. Mechanically activated ion channel Piezo1 modulates macrophage polarization and stiffness sensing[J]. Nat Commun. 2021;12(1):3256. https://doi.org/10.1038/s41467-021-23482-5.
12. Fang XZ, Li M, Wang YX, et al. Mechanosensitive ion channel Piezo1 mediates mechanical ventilation-exacerbated ARDS-associated pulmonary fibrosis[J]. J Adv Res. 2023;53:175–86. https://doi.org/10.1016/j.jare.2022.12.006.
13. Zhao X, Kong Y, Liang B, et al. Mechanosensitive Piezo1 channels mediate renal fibrosis[J]. JCI Insight. 2022;7(7). https://doi.org/10.1172/jci.insight.152330.
14. Braidotti N, Chen SN, Long CS, et al. Piezo1 channel as a potential target for hindering cardiac fibrotic Remodeling[J]. Int J Mol Sci. 2022;23(15). https://doi.org/10.3390/ijms23158065.
15. Shirane Y, Fujii Y, Ono A, et al. Peripheral T cell subpopulations as a potential surrogate biomarker during Atezolizumab plus bevacizumab treatment for hepatocellular Carcinoma[J]. Cancers (Basel). 2024;16(7). https://doi.org/10.3390/cancers16071328.
16. Tang H, Zeng R, He E, et al. Piezo-Type mechanosensitive ion channel component 1 (Piezo1): A promising therapeutic target and its Modulators[J]. J Med Chem. 2022;65(9):6441–53. https://doi.org/10.1021/acs.jmedchem.2c00085.
17. Kim H, Xue X. Detection of total reactive oxygen species in adherent cells by 2',7'-Dichlorodihydrofluorescein diacetate Staining[J]. J Vis Exp. 2020;16010.3791/60682.
18. Creed S, Mckenzie M. Measurement of mitochondrial membrane potential with the fluorescent dye tetramethylrhodamine Methyl ester (TMRM)[J]. Methods Mol Biol. 2019;1928:69–76. https://doi.org/10.1007/978-1-4939-9027-6_5.
19. Meyer EL, Jenkins C, Rengarajan K. NIH guidelines April 2019[J]. Appl Biosaf. 2019;24(4):179–81. https://doi.org/10.1177/1535676019871146.
20. Mo J, Gao Z, Zheng L, et al. Targeting mitochondrial one-carbon enzyme MTHFD2 together with pemetrexed confers therapeutic advantages in lung adenocarcinoma[J]. Cell Death Discov. 2022;8(1):307. https://doi.org/10.1038/s41420-022-01098-y.
21. Gines P, Krag A, Abraldes JG, et al. Liver cirrhosis[J]. Lancet. 2021;398(10308):1359–76. https://doi.org/10.1016/S0140-6736(21)01374-X.
22. Nagelkerke A, Bussink J, Rowan AE, et al. The mechanical microenvironment in cancer: how physics affects tumours[J]. Semin Cancer Biol. 2015;35:62–70. https://doi.org/10.1016/j.semcancer.2015.09.001.
23. Hasegawa K, Fujii S, Matsumoto S, et al. YAP signaling induces PIEZO1 to promote oral squamous cell carcinoma cell proliferation[J]. J Pathol. 2021;253(1):80–93. https://doi.org/10.1002/path.5553.
24. Chen X, Wanggou S, Bodalia A, et al. Neuron. 2018;100(4):799–815. https://doi.org/10.1016/j.neuron.2018.09.046. A Feedforward Mechanism Mediated by Mechanosensitive Ion Channel PIEZO1 and Tissue Mechanics Promotes Glioma Aggression[J].
25. Spier I, Kerick M, Drichel D, et al. Exome sequencing identifies potential novel candidate genes in patients with unexplained colorectal adenomatous polyposis[J]. Fam Cancer. 2016;15(2):281–8. https://doi.org/10.1007/s10689-016-9870-z.
26. Chen B, Liu X, Yu P, et al. H. pylori-induced NF-kappaB-PIEZO1-YAP1-CTGF axis drives gastric cancer progression and cancer-associated fibroblast-mediated tumour microenvironment remodelling[J]. Clin Transl Med. 2023;13(11):e1481. https://doi.org/10.1002/ctm2.1481.
27. Chen G, Gao X, Chen J, et al. Actomyosin activity and Piezo1 activity synergistically drive urinary system fibroblast Activation[J]. Adv Sci (Weinh). 2023;10(33):e2303369. https://doi.org/10.1002/advs.202303369.
28. Han Y, Liu C, Zhang D, et al. Mechanosensitive ion channel Piezo1 promotes prostate cancer development through the activation of the akt/mtor pathway and acceleration of cell cycle[J]. Int J Oncol. 2019;55(3):629–44. https://doi.org/10.3892/ijo.2019.4839.
29. Xu H, Chen Z, Li C. The prognostic value of Piezo1 in breast cancer patients with various clinicopathological features[J]. Anticancer Drugs. 2021;32(4):448–55. https://doi.org/10.1097/CAD.0000000000001049.
30. Huang Z, Sun Z, Zhang X, et al. Loss of stretch-activated channels, piezos, accelerates non-small cell lung cancer progression and cell migration[J]. Biosci Rep. 2019;39(3). https://doi.org/10.1042/BSR20181679.
31. Redza-Dutordoir M, Averill-Bates DA. Activation of apoptosis signalling pathways by reactive oxygen species[J]. Biochim Biophys Acta. 2016;1863(12):2977–92. https://doi.org/10.1016/j.bbamcr.2016.09.012.
32. Mo HY, Wang RB, Ma MY, et al. MTHFD2-mediated redox homeostasis promotes gastric cancer progression under hypoxic conditions[J]. Redox Rep. 2024;29(1):2345455. https://doi.org/10.1080/13510002.2024.2345455.
33. Zhang H, Zhu S, Zhou H, et al. Identification of MTHFD2 as a prognostic biomarker and ferroptosis regulator in triple-negative breast cancer[J]. Front Oncol. 2023;13:1098357. https://doi.org/10.3389/fonc.2023.1098357.
34. Achreja A, Yu T, Mittal A, et al. Metabolic collateral lethal target identification reveals MTHFD2 paralogue dependency in ovarian cancer[J]. Nat Metab. 2022;4(9):1119–37. https://doi.org/10.1038/s42255-022-00636-3.
35. Ramos L, Henriksson M, Helleday T, et al. Targeting MTHFD2 to exploit Cancer-Specific metabolism and the DNA damage Response[J]. Cancer Res. 2024;84(1):9–16. https://doi.org/10.1158/0008-5472.CAN-23-1290.
36. Yue L, Pei Y, Zhong L, et al. Mthfd2 modulates mitochondrial function and DNA repair to maintain the pluripotency of mouse stem Cells[J]. Stem Cell Rep. 2020;15(2):529–45. https://doi.org/10.1016/j.stemcr.2020.06.018.
37. Matsushima K, Yang D, Oppenheim JJ. Interleukin-8: an evolving chemokine[J]. Cytokine. 2022;153:155828. https://doi.org/10.1016/j.cyto.2022.155828.
38. Waugh DJ, Wilson C. The interleukin-8 pathway in cancer[J]. Clin Cancer Res. 2008;14(21):6735–41. 10.1158/1078– 0432.CCR-07-4843.
39. Ha H, Debnath B, Neamati N. Role of the CXCL8-CXCR1/2 Axis in Cancer and inflammatory Diseases[J]. Theranostics. 2017;7(6):1543–88. https://doi.org/10.7150/thno.15625.
40. Schalper KA, Carleton M, Zhou M, et al. Elevated serum interleukin-8 is associated with enhanced intratumor neutrophils and reduced clinical benefit of immune-checkpoint inhibitors[J]. Nat Med. 2020;26(5):688–92. https://doi.org/10.1038/s41591-020-0856-x.
41. Lavoie H, Gagnon J, Therrien M. ERK signalling: a master regulator of cell behaviour, life and fate[J]. Nat Rev Mol Cell Biol. 2020;21(10):607–32. https://doi.org/10.1038/s41580-020-0255-7.

42. He Y, Sun MM, Zhang GG, et al. Targeting PI3K/Akt signal transduction for cancer therapy[J]. Signal Transduct Target Ther. 2021;6(1):425. https://doi.org/10.1038/s41392-021-00828-5.
43. Abdel-Rahman O. Revisiting oxaliplatin-based regimens for advanced hepatocellular carcinoma[J]. Curr Oncol Rep. 2014;16(8):394. https://doi.org/10.1007/s11912-014-0394-0.
44. Bae C, Sachs F, Gottlieb PA. The mechanosensitive ion channel Piezo1 is inhibited by the peptide GsMTx4[J]. Biochemistry. 2011;50(29):6295–300. https://doi.org/10.1021/bi200770q.
45. Badimon L, Vilahur G, Rocca B, et al. The key contribution of platelet and vascular arachidonic acid metabolism to the pathophysiology of atherothrombosis. Cardiovasc Res. 2015;117(9):2001. https://doi.org/10.1093/cvr/cvab003.
46. Wang B, Wu L, Chen J et al. Metabolism pathways of arachidonic acids: mechanisms and potential therapeutic targets. Signal Transduct Target Ther, 6(1): 94. https://doi.org/10.1038/s41392-020-00443-w
47. Romero LO, Massey AE, Mata-Daboin AD et al. Dietary fatty acids fine-tune Piezo1 mechanical response. Nat Commun, 10(1):1200. https://doi.org/10.1038/s41467-019-09055-7

Publisher's note